UNIVERSITY OF CAMBRIDGE
Faculty of Economics

Institute for
New Economic Thinking

CAMBRIDGE WORKING PAPERS IN ECONOMICS
CAMBRIDGE-INET WORKING PAPERS

Matching Theory and Evidence on Covid-19 using a Stochastic Network SIR Model

M. Hashem Pesaran
University of Southern California

Cynthia Fan Yang
Florida State University

Abstract

This paper develops an individual-based stochastic network SIR model for the empirical analysis of the Covid-19 pandemic. It derives moment conditions for the number of infected and active cases for single as well as multigroup epidemic models. These moment conditions are used to investigate identification and estimation of recovery and transmission rates. The paper then proposes simple moment-based rolling estimates and shows them to be fairly robust to the well-known under-reporting of infected cases. Empirical evidence on six European countries match the simulated outcomes, once the under-reporting of infected cases is addressed. It is estimated that the number of reported cases could be between 3 to 9 times lower than the actual numbers. Counterfactual analysis using calibrated models for Germany and UK show that early intervention in managing the infection is critical in bringing down the reproduction numbers below unity in a timely manner.

Reference Details

20102 Cambridge Working Papers in Economics
2020/48 Cambridge-INET Working Paper Series

Published 11 November 2020

Key Words Covid-19, multigroup SIR model, basic and effective reproduction numbers, rolling window estimates of the transmission rate, method of moments, calibration and counterfactual analysis

JEL Codes C13, C15, C31, D85, I18, J18

Websites www.econ.cam.ac.uk/cwpe
www.inet.econ.cam.ac.uk/working-papers

Matching Theory and Evidence on Covid-19 using a Stochastic Network SIR Model*

M. Hashem Pesaran

University of Southern California, USA, and Trinity College, Cambridge, UK

Cynthia Fan Yang

Florida State University

November 10, 2020

Abstract

This paper develops an individual-based stochastic network SIR model for the empirical analysis of the Covid-19 pandemic. It derives moment conditions for the number of infected and active cases for single as well as multigroup epidemic models. These moment conditions are used to investigate identification and estimation of recovery and transmission rates. The paper then proposes simple moment-based rolling estimates and shows them to be fairly robust to the well-known under-reporting of infected cases. Empirical evidence on six European countries match the simulated outcomes, once the under-reporting of infected cases is addressed. It is estimated that the number of reported cases could be between 3 to 9 times lower than the actual numbers. Counterfactual analysis using calibrated models for Germany and UK show that early intervention in managing the infection is critical in bringing down the reproduction numbers below unity in a timely manner.

Keywords: Covid-19, multigroup SIR model, basic and effective reproduction numbers, rolling window estimates of the transmission rate, method of moments, calibration and counterfactual analysis.

JEL Classifications: C13, C15, C31, D85, I18, J18

*We appreciate helpful comments from Alexander Chudik, Cheng Hsiao, Ron Smith, and participants at the 2020 IAAE webinar series. We would like to thank Mahrad Sharifvaghefi for helping us compile the data, and Minsoo Cho for helping with the literature review. Correspondence to: C.F. Yang, Department of Economics, Florida State University, 281 Bellamy Building, Tallahassee, FL 32306, USA. E-mail: cynthia.yang@fsu.edu.

1 Introduction

Since the outbreak of Covid-19, many researchers in epidemiology, behavioral sciences and economics have applied various forms of compartmental models to study the disease transmission and potential outcomes under different intervention policies. The compartmental models are a major group of epidemiological models that categorize a population into several types or groups, such as susceptible (S), infected (I), and removed (or recovered, R). Compartmental models owe their origin to the well-known SIR model pioneered by Kermack and McKendrick (1927), and have been developed in a number of important directions, allowing for multi-category (multi-location), a variety of contact networks and transmission channels.

In this paper we follow the individual-based modelling approach and develop a stochastic network SIR model in which individual-specific infection and recovery processes are modelled, allowing for group heterogeneity and latent individual characteristics that distinguish individuals in terms of their degrees of resilience to becoming infected. The model is then used to derive individual-specific conditional probabilities of infection and recovery. In this respect our modelling approach is to be distinguished from the individual-based models in epidemiology that specify the transition probabilities of individuals from one state to another. In modelling the infection process we consider an individual's contact pattern with others in the network, plus an individual-specific latent factor assumed to be exponentially distributed. The time from infection to recovery (or death) is assumed to be geometrically distributed. The individual processes are shown to aggregate up to the familiar multigroup SIR model. We allow for group heterogeneity and, in line with the literature, assume contact probabilities are homogeneous within groups but could differ across groups.

We then derive the probabilities of individuals within a given group being in a particular state at a given time, conditional on contact patterns, exposure intensities, and unobserved characteristics. These conditional probabilities are aggregated up to form a set of moment conditions that can be taken to the data on the number of infected and active cases both at the aggregate and group (or regional) levels. We make use of the moment conditions to investigate the identification

of the underlying structural parameters and most importantly show that, whilst one can not distinguish between average contact numbers and the degree of exposure to the virus upon contact, it is nevertheless possible to identify the basic and effective reproduction numbers from relatively short time series observations on infections and recoveries. Using Monte Carlo simulations, the small sample properties of the proposed estimator are shown to be satisfactory, with a high degree of precision even when using 2 or 3 weeks of rolling observations. Most importantly, they are quite robust to the well-known under-reporting of infected cases. Equipped with daily estimates of the transmission rates we are then able to calibrate our epidemic model and investigate its properties under different network topology, population sizes, and group numbers, as well as different types of interventions that are aimed to alter the transmission rates through policy.

We also apply our estimation approach to examine how well the outcome of the proposed epidemic model matches the Covid-19 evidence in the case of six European countries (Austria, France, Germany, Italy, Spain, and United Kingdom) from March to October 15, 2020. We provide rolling estimates of the transmission rates and related effective reproduction numbers using the recorded infected cases and show that the estimates are fairly robust to the under-reporting of the number of infected cases. We then use the estimated transmission rates to calibrate our SIR network model parameters across the six countries. The stochastically simulated outcomes are shown to be reasonably close to the reported cases once the under-reporting issue is taken into account. We estimate that the number of reported infected cases could be 3 to 9 times lower than the true number of infections across the six European countries under consideration. It is also of interest that our model allows us to capture the second surge of Covid-19 cases that European countries began to experience starting August 2020.

Finally, the paper develops a new way of using the modelling of epidemics for counterfactual inference. We use the calibrated model to investigate the potential outcomes if the lockdown in Germany had been delayed for one or two weeks; and if the lockdown in the UK had started one or two weeks earlier. Such counterfactual analyses can be achieved by shifting the estimated transmission rates forward or backward. We show that early intervention is critical in managing the infection and controlling the total number of infected and active cases.

The problem of how to balance the public health risks from the spread of the epidemic with the economic costs associated with lockdowns and other social-distancing mandated policies will not be addressed in this paper. However, the proposed network SIR model with its individual-based architecture is eminently suited to this purpose. The proposed model can be combined with behavioral assumptions about how individuals trade off infection risk and economic well being, thus generalizing the aggregate framework proposed in Chudik, Pesaran, and Rebucci (2020) to individual-based SIR models.

The rest of the paper is organized as follows. Section 2 reviews the related literature. Section 3 introduces the basic concepts and the classical multigroup SIR model. Section 4 lays out our individual based stochastic model on a network. Section 5 explains the calibration of our model to basic and effective reproduction numbers. Section 6 documents the properties of the model. Sections 7 and 8 discuss the estimation of the transmission rate and recovery rate, respectively. Section 9 presents the calibration of the model to Covid-19 evidence and counterfactual analyses, and Section 10 concludes. The Online Supplement provides some technical derivations and presents additional simulation results.

2 Related literature

Our modelling approach relates to two important strands of the literature on mathematical modelling of infectious diseases, namely the classical SIR model due to Kermack and McKendrick (1927) and its various extensions to multigroup SIR models, and the individual-based network models. The multigroup SIR model allows for a heterogeneous population where each compartment (S, I or R) is further partitioned into multiple groups based on one or more factors including age, gender, location, contact patterns, and a number of economic and social factors. One of the earliest multigroup models was pioneered by Lajmanovich and Yorke (1976), who developed a class of SIS (susceptible-infected-susceptible) models for the transmission of gonorrhea. Subsequent extensions to the multigroup SIR model and its variants include Hethcote (1978), Thieme (1983, 1985), Beretta and Capasso (1986), and many others. Reviews of multigroup models can be

found in Hethcote (2000) and Thieme (2013). In contrast, we do not model the progression of epidemics at the compartment level; instead, we develop an individual-based stochastic model from which we derive a set of aggregate moment conditions. Interestingly, we are able to show that the multigroup SIR model can be derived as a linearized-deterministic version of our individual-based stochastic model.

Our analysis also relates to the more recent literature on mathematical models of epidemics on networks, whereby the spread of the epidemic is modelled via networks (or graphs), with nodes representing single individuals or groups of individuals and links (or edges) representing contacts. The adoption of networks in epidemiology has opened up a myriad of possibilities, using more realistic contact patterns to investigate the impact of network structure on epidemic outcomes, and to design network-based interventions. Kiss, Miller, and Simon (2017) provide a systematic treatment of this literature, with related reviews in Miller and Kiss (2014) and Pastor-Satorras et al. (2015).

Being based on individual outcomes, our approach is more closely related to the individual-based models surveyed by Willem et al. (2017) and Nepomuceno, Resende, and Lacerda (2018). These models consider the transition probability of individuals from one state (S,I,R) to another (Rocha and Masuda, 2016). In contrast, as noted in the introduction, we do not model the transition probabilities, but rather we model the contact probabilities and unobserved individual-specific probability of becoming infected, and then derive individual-specific transition probabilities. Like the individual-based models, our approach also allows for considerable group heterogeneity and has the advantage that aggregates up to the multigroup SIR model.

In order to calibrate the average number of contacts in our model, we drew upon the literature on social contact patterns relevant to the transmission of respiratory infectious diseases. Before the outbreak of Covid-19, large-scale social contact surveys have been conducted in many countries aiming to guide effective policies on infectious disease control and prevention.[1] The POLYMOD study of social contacts in eight European countries by Mossong et al. (2008) is a notable land-

[1] Summaries of these social contact surveys are provided by Hoang et al. (2019) and Supplementary Table S1 of Leung et al. (2017).

mark.[2] Many similar surveys have been conducted since. Among them, the contact studies in Hong Kong (Leung et al., 2017) and Shanghai (Zhang et al., 2019) provide valuable information about the pre-Covid social contacts in China. Most of these studies summarize contact patterns based on age groups, contact locations (e.g. households, schools, workplaces), and time schedule (e.g. weekday or weekend) that can be utilized in a multigroup epidemiological models. With the outbreak of Covid-19, a few recent articles reported significant changes in contact patterns. For example, Zhang et al. (2020a) find that the median number of daily contacts in Wuhan went down from 7 in normal times to 2 after the Covid-19 outbreak. The median number of daily contacts in Shanghai fell from 10 to 2. Jarvis et al. (2020) find that the average daily number of contacts declined from 10.8 in normal times to 2.8 immediately after the lockdown in the UK. In all these three cases, the contact number by age flattened after the outbreak.

In this paper, we propose a new method of estimating the transmission rate, β_t, using the moment conditions we derive from our stochastic network SIR model. The transmission rate is closely connected to the reproduction numbers, which are epidemiologic metrics used to measure the intensity of an infectious disease. The basic reproduction number, denoted by $\mathcal{R}_0$, is the number of new infections expected to result from one infected individual at the start of the epidemic, and within SIR models it is defined by $\mathcal{R}_0 = \beta_0/\gamma$, where β_0 is the initial transmission rate, and γ is the recovery rate. For the current Covid-19, estimates of $\mathcal{R}_0$ range between 2 to 3.[3] Since the transmissibility of a disease will vary over time due to changes in immunity and/or mitigation policies, the effective reproduction number, which we denote by $\mathcal{R}_{et}$, measures the $\mathcal{R}$ number t periods after the initial outbreak. The effective $\mathcal{R}$ number is governed by the extent to which the susceptible population is shrinking and the effectiveness of mitigation policies (whether mandated or voluntary). In the single group SIR model we have $\mathcal{R}_{et} = (1 - c_t)\,\beta_t/\gamma$, where c_t is the per capita number of infected cases at time t.

Various methods are available in the epidemiological literature to estimate the reproduction numbers at the beginning and/or in real time during epidemics, but there is no uniform framework.

[2] The eight countries are Belgium, Germany, Finland, Great Britain, Italy, Luxembourg, The Netherlands, and Poland.

[3] A summary of published $\mathcal{R}_0$ values is provided in Table 1 of D'Arienzo and Coniglio (2020).

Estimation approaches, that are data-driven and involve simplifying assumptions, include the use of the number of susceptibles at endemic equilibrium, the average age at infection, the final size equation, and calculation from the intrinsic growth rate of the number of infections (Heffernan, Smith, and Wahl, 2005). Estimation of reproduction numbers based on different mathematical models are reviewed by Chowell and Nishiura (2008), Obadia, Haneef, and Boëlle (2012), and Nikbakht et al. (2019). More recent contributions, focusing on estimation of reproduction numbers for the Covid-19 pandemic include Atkeson, Kopecky, and Zha (2020), Baqaee et al. (2020), Fernández-Villaverde and Jones (2020), Korolev (2020) and Toda (2020).

In this paper we estimate the transmission rate using the moment conditions derived from our stochastic individual-based network SIR epidemic model. We do not use mortality data due to its unreliability,[4] but instead our method of moment estimation requires only data on per capita infected cases. Our estimation method is not only simple to apply, but also fairly robust to the under-reporting of infected cases. It has been widely acknowledged that the reported infected cases may suffer from considerable under-reporting, especially during the early stages of the epidemic. Li et al. (2020) estimate that only 14 percent of all infections were documented in China prior to the January 23, 2020 travel restrictions. This translates to a multiplication factor of $1/0.14 \approx 7.14$, which is a quantity that measures the degree of under-reporting and will be elaborated in later sections of our paper. Jagodnik et al. (2020) estimate that the recorded cases were under-reported by a multiplication factor in the range of 3 to 16 times in seven countries as of March 28, 2020.[5] In the US, the number of infected cases is likely to be 10 times more than reported based on antibody tests from March through May, according to the study by Havers et al. (2020) led by the Centers for Disease Control and Prevention (CDC). More recently, Rahmandad, Lim, and Sterman (2020) estimate that the cumulative cases across 86 countries through July 10, 2020 are 10.5 times the number of official reported cases, with $10^{th} - 90^{th}$ percentile range $3.35 - 23.81$. Another source of measurement errors is reporting delays. Harris (2020) estimates that in New

[4]The recorded Covid death toll has undergone major revisions on several occasions. For example, the UK death toll was revised downwards by 5,377 on August 12, 2020 after a review concluded the daily death figure should only include deaths which had occurred within 28 days of a positive test.

[5]See Table 2 of Jagodnik et al. (2020). The seven countries considered are China, France, Italy, Spain, US, Germany and UK.

York City the mean delay in reporting was 5 days, with 15 percent of cases reported after 10 or more days, during June 21–August 1, 2020. Many existing estimation methods of reproduction numbers do not allow for measurement errors and might not be robust to acknowledged under-reporting errors. For instance, the SUR estimates developed by Korolev (2020) may be biased downward if one neglects under-reporting of confirmed cases.

Our study also contributes to a growing literature on quantitative epidemic policy analyses. A number of studies consider the effects of different intervention strategies (such as isolating the elderly, closing schools and/or workplaces, and alternating work/school schedules) by hypothetically lowering the average number of contacts of some specific age groups, and/or contact locations/schedules from normal (pre-Covid) levels using SIR or other compartmental models. (See Acemoglu et al. (2020), Akbarpour et al. (2020), Matrajt and Leung (2020), among others.) Chudik et al. (2020) simulate the trade-off between flattening the epidemic curves and lessening unemployment loss under different degrees of mandatory and voluntary social distancing policies using a modified SIR model. Toda (2020) simulates the effects of different mitigation policies on epidemic curves by reducing the transmission rate in the SIR model from its initial level. Atkeson et al. (2020) investigate the impact of earlier or later mitigation measures on the death toll. Our model can be used to investigate a number of different mitigation policies either by lowering the number of contacts across age groups and/or by reducing the rate of infection upon contact. In the present paper we have focused on the timing of the lockdowns, comparing the spread of Covid-19 in UK and Germany in March 2020. But the model can be used in a variety of other contexts.

3 Basic concepts and the multigroup SIR model

We consider a population of n individuals that are subject to the spread of a disease with some initially infected individuals. We suppose that the susceptible population can be categorized into L groups of size n_ℓ, $\ell = 1, 2, \ldots, L$, with L fixed. $n = \sum_{\ell=1}^{L} n_\ell$, with $w_\ell = n_\ell/n > 0$, for all n and as $n \to \infty$. The grouping could be based on demographic factors (age and/or gender), or other observed characteristics such as contact locations and/or schedules, mode of transmission,

genetic susceptibility, group-specific vaccination coverage, as well as socioeconomic factors. See, for example, Hethcote (2000). Individual i in group ℓ will be referred to as individual (i, ℓ), with $i = 1, 2, \ldots, n_\ell$ and $\ell = 1, 2, \ldots, L$. It is assumed that n_ℓ is relatively large but remains fixed over the course of the epidemic measured in days.

Suppose that individual (i, ℓ) becomes infected on day $t = t^*_{i\ell}$, and let $x_{i\ell,t}$ to take the value of unity for all $t \geq t^*_{i\ell}$, and zero otherwise. In this way, we follow the convention that once an individual becomes infected, he/she is considered as infected thereafter, irrespective of whether that individual recovers or dies. Specifically, we set

$$x_{i\ell,t} = 0, \text{ for all } t < t^*_{i\ell}; \quad \text{and} \quad x_{i\ell,t} = 1, \text{ for all } t \geq t^*_{i\ell}. \tag{1}$$

The event of recovery or death of individual (i, ℓ) at time t will be represented by $y_{i\ell,t}$, which will be equal to zero unless the individual is "removed" (recovered or dead). An individual (i, ℓ) is considered to be "active" if he/she is infected and not yet recovered. We denote the active indicator by $z_{i\ell,t}$, which is formally defined by

$$z_{i\ell,t} = (1 - y_{i\ell,t})\, x_{i\ell,t}. \tag{2}$$

$z_{i\ell,t}$ takes the value of 0 if individual (i, ℓ) has not been infected, or has been infected but recovered/dead. It takes the value of 1 if he/she is infected and not yet recovered. Any individual (i, ℓ) who has not been infected is viewed "susceptible" and indicated by $s_{i\ell,t} = 1$, where

$$s_{i\ell,t} = 1 - z_{i\ell,t} - y_{i\ell,t}. \tag{3}$$

It then readily follows that the total (cumulative) number of those "infected" in group ℓ at the end of day t is given by

$$C_{\ell t} = \sum_{i=1}^{n_\ell} x_{i\ell,t}, \ \ell = 1, 2, \ldots, L, \tag{4}$$

where the summation is over all individuals in group ℓ. The total number of "recovered" in group

ℓ in day t is given by

$$R_{\ell t} = \sum_{i=1}^{n_\ell} y_{i\ell,t},\ \ell = 1, 2, \ldots, L. \tag{5}$$

The total number of "active" cases (individuals who are infected and not yet removed) in group ℓ in day t is

$$I_{\ell t} = \sum_{i=1}^{n_\ell} z_{i\ell,t} = \sum_{i=1}^{n_\ell} x_{i\ell,t} - \sum_{i=1}^{n_\ell} x_{i\ell,t} y_{i\ell,t} = C_{\ell t} - R_{\ell t}. \tag{6}$$

The number of "susceptible" individuals in group ℓ in day t is

$$S_{\ell t} = \sum_{i=1}^{n_\ell} s_{i\ell,t} = n_\ell - I_{\ell t} - R_{\ell t}. \tag{7}$$

Our model does not distinguish between recovery and death. Once an individual is removed (recovered or dead), following the SIR literature we assume that he/she cannot be infected again. Under this assumption, recovery and death have the same effects on the evolution of the epidemic, and accordingly in what follows we shall not distinguish between recovery and death and refer to their total as "removed".[6]

The classic multigroup SIR model in discretized form can be written as[7]

$$S_{\ell,t+1} - S_{\ell t} = -S_{\ell t} \sum_{\ell'=1}^{L} \beta_{\ell\ell'} I_{\ell' t}, \tag{8}$$

$$I_{\ell,t+1} - I_{\ell t} = S_{\ell t} \sum_{\ell'=1}^{L} \beta_{\ell\ell'} I_{\ell' t} - \gamma_\ell I_{\ell t} \tag{9}$$

$$R_{\ell,t+1} - R_{\ell t} = \gamma_\ell I_{\ell t}, \tag{10}$$

for $\ell = 1, 2, \ldots, L$ and $t = 1, 2, \ldots, T$, where $S_{\ell t}$, $I_{\ell t}$ and $R_{\ell t}$ are defined as above, γ_ℓ is the recovery rate which is assumed to be time-invariant and the same for all people in group ℓ, and $\beta_{\ell\ell'}$ is the transmission coefficient between $S_{\ell t}$ and $I_{\ell' t}$. Note that individuals in group ℓ' may transmit the contagion to individuals in group ℓ, with the new infections in group ℓ given by $S_{\ell t} \sum_{\ell'=1}^{L} \beta_{\ell\ell'} I_{\ell' t}$.[8]

[6] Although it is also possible to calibrate our model using mortality data, we do not pursue this route as it is well known that it is difficult to correctly attribute deaths to Covid-19.

[7] See, for example, Guo, Li, and Shuai (2006) and Zhang et al. (2020b) and the references therein.

[8] For some of the recent contributions in the epidemiological literature on the multigroup SIR models and their stability conditions, see, for example, Hyman, Li, and Stanley (1999), Guo, Li, and Shuai (2006), Li, Shuai, and

4 An individual based stochastic epidemic model on a network

We depart from the literature by explicitly modelling the individual indicators, $x_{i\ell,t}$ and $y_{i\ell,t}$, (and hence $z_{i\ell,t}$) and then simulate and aggregate up to match the theory predictions with realized outcomes. In this section, we first describe the infection and recovery processes at individual level, then show how they lead to the moment conditions at group levels, and finally derive the relation between aggregated outcomes from our model and the multigroup SIR model.

4.1 Modelling the infection and recovery processes

As an attempt to better integrate individual decisions to mitigate their health risk within the epidemic model we propose to directly model $x_{i\ell,t}$ for each individual (i,ℓ), as compared to modelling the group aggregates $S_{\ell t}$, $R_{\ell t}$, and $I_{\ell t}$. We follow the micro-econometric literature and model the infection process using the latent variable, $x^*_{i\ell,t+1}$, which determines whether individual (i,ℓ) becomes infected. Specifically we begin with the following Markov switching process for individual (i,ℓ):

$$x_{i\ell,t+1} = x_{i\ell,t} + (1 - x_{i\ell,t})\, I\left(x^*_{i\ell,t+1} > 0\right), \tag{11}$$

where $I(\mathcal{A})$ is the indicator function that takes the value of unity if $\mathcal{A} > 0$, and zero otherwise. We suppose that $x^*_{i\ell,t+1}$ is composed of two different components. The first component relates to the contact pattern of individual (i,ℓ) with all other individuals in the active set, denoted by $z_{j\ell',t}$, both within (when $\ell' = \ell$) and outside of his/her group (when $\ell' \neq \ell$). The second component is an unobserved individual-specific infection threshold variable, $\xi_{i\ell,t+1}$. Formally, we set

$$x^*_{i\ell,t+1} = \tau_\ell \sum_{\ell'=1}^{L} \sum_{j=1}^{n_{\ell'}} d_{i\ell,j\ell'}(t)\, z_{i\ell',t} - \xi_{i\ell,t+1}, \tag{12}$$

where the first component depends on pattern of contacts, $d_{i\ell,j\ell'}(t)$, whether the contacted individuals are infectious, $z_{j\ell',t}$, and the exposure intensity parameter, denoted by τ_ℓ. $\mathbf{D}(t) = \left[d_{i\ell,j\ell'}(t)\right]$ is

Wang (2010), Ji, Jiang, and Shi (2011), Ding, Qin, and Ding (2015) and Zhou, Yang, and Zhang (2017).

the contact network matrix, such that $d_{i\ell,j\ell'}(t) = 1$ if individual (i,ℓ) is in contact with individual $\left(j,\ell'\right)$ at time t. $z_{i\ell',t} = (1 - y_{i\ell',t})\, x_{i\ell',t}$ is an infectious indicator, already defined by (2), and takes the value of unity if individual (j,ℓ') is infected and not yet recovered, zero otherwise. The exposure intensity parameter, τ_ℓ, is group-specific and depends on the average duration of contacts, whether the contacting individuals are wearing facemasks, and if they follow other recommended precautions.

The multigroup structure of the first component of (12) covers a wide range of observable characteristics, and can be extended to allow for differences in age, location, and medical preconditions. There are also many unobservable characteristics which lead to different probabilities of infection even for individuals with the same contact patterns and exposure intensities. To allow for such latent factors, we have introduced the individual-specific positive random variable $(\xi_{i\ell,t+1} > 0)$ which represents the individual's degree of resilience to becoming infected and varies across (i,ℓ) and t. *Ceteris paribus*, an individual with a low value of $\xi_{i\ell,t+1}$ is more likely to become infected. $\xi_{i\ell,t+1}$ is assumed to be independently distributed over i, ℓ and t, and follows an exponential distribution with the cumulative distribution function given by

$$\Pr\left(\xi_{i\ell,t+1} < a\right) = 1 - \exp\left(-\mu_\ell^{-1} a\right), \quad \text{for } a \geq 0, \tag{13}$$

where $\mu_\ell = E\left(\xi_{i\ell,t+1}\right)$. As we shall see, it is not possible to distinguish between μ_ℓ and τ_ℓ.

To complete the specification of the infection process we also need to model $y_{i\ell,t}$, namely the recovery indicator. We assume that recovery depends on the number of days since infection. Specifically, the recovery process for individual i is defined by

$$y_{i\ell,t+1} = y_{i\ell,t} + z_{i\ell,t}\ \zeta_{i\ell,t+1}\left(t_{i\ell}^*\right), \tag{14}$$

where $z_{i\ell,t} = (1 - y_{i\ell,t})\, x_{i\ell,t}$, $\zeta_{i\ell,t+1}\left(t_{i\ell}^*\right) = 1$ if individual (i,ℓ) recovers at time $t+1$, having been infected exactly at time $t_{i\ell}^*$ and not before, and $\zeta_{i\ell,t+1}\left(t_{i\ell}^*\right) = 0$, otherwise. The analysis of recovery simplifies considerably if we assume time to removal, denoted by $T_{i\ell,t}^* = t - t_{i\ell}^*$, follows

the geometric distribution (for $t - t^*_{i\ell} = 1, 2, \ldots$)

$$\Pr\left[\zeta_{i\ell,t+1}\left(t^*_{i\ell}\right) = 1\right] = \Pr\left(T^*_{i\ell,t} = t - t^*_{i\ell}\right) = \gamma_\ell \left(1 - \gamma_\ell\right)^{t - t^*_{i\ell} - 1}.$$

Then

$$\begin{aligned}
&E\left[\zeta_{i\ell,t+1}\left(t^*_{i\ell}\right) \middle| x_{i\ell,t}, y_{i\ell,t}, y_{i\ell,t-1}, \ldots, y_{i\ell,t^*_{i\ell}}\right] \\
&= \Pr\left[\zeta_{i\ell,t+1}\left(t^*_{i\ell}\right) = 1 \,|x_{i\ell,t} = 1, y_{i\ell,s} = 0, \text{ for } t^*_{i\ell} \leq s \leq t\right] \\
&= \frac{\Pr\left[\zeta_{i\ell,t+1}\left(t^*_{i\ell}\right) = 1\right]}{1 - \Pr\left[y_{i\ell,s} = 0, s = t^*_{i\ell} + 1, t^*_{i\ell} + 2, \ldots, t\right]} \\
&= \frac{\Pr\left(T^*_{i\ell,t} = t - t^*_{i\ell}\right)}{\Pr\left(T^*_{i\ell,t} > t - t^*_{i\ell} - 1\right)},
\end{aligned} \tag{15}$$

which is the probability of recovery at time $t+1$ having remained infected for $t - t^*_{i\ell} - 1$ days. As is well known this is the "hazard function" given by

$$h_\ell\left(t - t^*_{i\ell}\right) = \frac{\Pr\left(T^*_{i\ell,t} = t - t^*_{i\ell}\right)}{\Pr\left(T^*_{i\ell,t} > t - t^*_{i\ell} - 1\right)} = \frac{\gamma_\ell \left(1 - \gamma_\ell\right)^{t - t^*_{i\ell} - 1}}{\left(1 - \gamma_\ell\right)^{t - t^*_{i\ell} - 1}} = \gamma_\ell, \tag{16}$$

which is the same across all individuals within a given group, and which most importantly does not depend on the number of days since infection.[9] Therefore, using (15) and (16) in (14), the recovery micro-moment condition simplifies to

$$E\left(y_{i\ell,t+1} \,|y_{i\ell,t}, z_{i\ell,t}\right) = y_{i\ell,t} + \gamma_\ell \; z_{i\ell,t}. \tag{17}$$

We assume that $d_{i\ell,j\ell'}(t)$, the elements of the $n \times n$ network matrix $\mathbf{D}(t) = \left(d_{i\ell,j\ell'}(t)\right)$ are independent draws with $E\left[d_{i\ell,j\ell'}(t)\right] = p_{\ell\ell'}$, namely, the probability of contacts is homogeneous within groups but differs across groups. Let $\boldsymbol{d}_i'(t)$ be the i^{th} row of $\mathbf{D}(t)$. Also let $\mathbf{z}_t$ be a column

[9] A more general specification that allows the recovery probability to depend on the number of days being infected is considered in Section S1 of the Online Supplement.

vector consisting of $z_{j\ell,t}$, for $j = 1, 2, \ldots, n_\ell$ and $\ell = 1, 2, \ldots, L$. Then using (11) we have

$$\begin{aligned} E\left[x_{i\ell,t+1}|x_{i\ell,t},\ \mathbf{z}_t,\ \boldsymbol{d}_i\left(t\right)\right] &= x_{i\ell,t} + \left(1 - x_{i\ell,t}\right) \Pr\left[x^*_{i\ell,t+1} > 0|\ \boldsymbol{z}_t,\ \boldsymbol{d}_i\left(t\right)\right] \\ &= x_{i\ell,t} + \left(1 - x_{i\ell,t}\right) \Pr\left[\xi_{i\ell,t+1} < \tau_\ell \sum_{\ell'=1}^{L} \sum_{j=1}^{n_{\ell'}} d_{i\ell,j\ell'}\left(t\right) z_{j\ell',t}\right] \\ &= x_{i\ell,t} + \left(1 - x_{i\ell,t}\right) \left\{1 - \exp\left[-\left(\tau_\ell/\mu_\ell\right) \sum_{\ell'=1}^{L} \sum_{j=1}^{n_{\ell'}} d_{i\ell,j\ell'}\left(t\right) z_{j\ell',t}\right]\right\}. \end{aligned}$$

It is clear that τ_ℓ and μ_ℓ are not separately identified. Without loss of generality, in what follows we set $\mu_\ell = 1$. Since in general individual contact patterns are not observed, we also need to derive $E\left(x_{i\ell,t+1}|x_{i\ell,t}, \mathbf{z}_t\right)$. To this end we first note that

$$\begin{aligned} & E\left\{\exp\left[-\tau_\ell d_{i\ell,j\ell'}\left(t\right) z_{j\ell',t}\right] \mid \mathbf{z}_t\right\} \\ &= \exp\left(0\right) \Pr\left[d_{i\ell,j\ell'}\left(t\right) = 0\right] + \exp\left(-\tau_\ell z_{j\ell',t}\right) \Pr\left[d_{i\ell,j\ell'}\left(t\right) = 1\right] \\ &= 1 - p_{\ell\ell'} + \exp\left(-\tau_\ell z_{j\ell',t}\right) p_{\ell\ell'}, \end{aligned}$$

and since by assumption $d_{i\ell,j\ell'}\left(t\right)$ are independently distributed, we then have

$$\begin{aligned} E\left(x_{i\ell,t+1}|\ \mathbf{z}_t\right) &= x_{i\ell,t} + \left(1 - x_{i\ell,t}\right) \left\{1 - E\left[\exp\left(-\tau_\ell \sum_{\ell'=1}^{L} \sum_{j=1}^{n_{\ell'}} d_{i\ell,j\ell'}\left(t\right) z_{j\ell',t}\right)\right]\right\} \\ &= 1 - \left(1 - x_{i\ell,t}\right) \prod_{\ell'=1}^{L} \prod_{j=1}^{n_{\ell'}} \left[1 - p_{\ell\ell'} + \exp\left(-\tau_\ell z_{j\ell',t}\right) p_{\ell\ell'}\right]. \end{aligned}$$

However, recall that $z_{j\ell',t} = 1$ if individual (j, ℓ') is currently infected (namely if at time t he/she is a member of the active set, $\mathcal{I}_t$), otherwise $z_{j\ell',t} = 0$. In the latter case $1 - p_{\ell\ell'} + \exp\left(-\tau_\ell z_{j\ell',t}\right) p_{\ell\ell'} = 1$, and hence

$$\begin{aligned} E\left(x_{i\ell,t+1}|\ \mathbf{z}_t\right) &= 1 - \left(1 - x_{i\ell,t}\right) \prod_{\ell'=1}^{L} \left[\prod_{j=1, z_{j\ell',t}=1}^{n_{\ell'}} \left(1 - p_{\ell\ell'} + p_{\ell\ell'} e^{-\tau_\ell}\right)\right] \\ &= 1 - \left(1 - x_{i\ell,t}\right) \prod_{\ell'=1}^{L} \left(1 - p_{\ell\ell'} + p_{\ell\ell'} e^{-\tau_\ell}\right)^{I_{\ell' t}}, \end{aligned} \tag{18}$$

where $I_{\ell' t} = \sum_{j=1}^{n_{\ell'}} z_{j\ell',t} = C_{\ell' t} - R_{\ell' t}$. See also (6).

4.2 Moment conditions at group and aggregate levels

Aggregating the micro infection moment conditions, (18), over i for a given group ℓ, we obtain

$$E\left(\sum_{i=1}^{n_\ell} x_{i\ell,t+1}|\ \mathbf{z}_t\right) = E\left(C_{\ell,t+1}|\ \mathbf{z}_t\right) = n_\ell - (n_\ell - C_{\ell t}) \prod_{\ell'=1}^{L} \left(1 - p_{\ell\ell'} + p_{\ell\ell'} e^{-\tau_\ell}\right)^{I_{\ell' t}},$$

which can be written equivalently as (recall that $I_{\ell t} = C_{\ell t} - R_{\ell t}$)

$$E\left(C_{\ell,t+1} - C_{\ell t}|\ \mathbf{I}_t\right) = (n_\ell - C_{\ell t}) \left[1 - \prod_{\ell'=1}^{L} \left(1 - p_{\ell\ell'} + p_{\ell\ell'} e^{-\tau_\ell}\right)^{C_{\ell' t} - R_{\ell' t}}\right], \text{ for } \ell = 1, 2, \ldots, L, \quad (19)$$

where $\mathbf{I}_t = (I_{1t}, I_{2t}, \ldots, I_{Lt})'$. Also aggregating the micro recovery moment conditions, (17), we have

$$E\left(R_{\ell,t+1}|R_{\ell t}, C_{\ell t}\right) = (1 - \gamma_\ell) R_{\ell,t} + \gamma_\ell C_{\ell t}, \text{ for } \ell = 1, 2, \ldots, L. \quad (20)$$

In per capita terms we obtain the following $2L$ dimensional system of moment conditions (for $\ell = 1, 2, \ldots, L$)

$$E\left(\frac{1 - c_{\ell,t+1}}{1 - c_{\ell t}}|\ \mathbf{i}_t\right) = \prod_{\ell'=1}^{L} \left(1 - p_{\ell\ell'} + p_{\ell\ell'} e^{-\tau_\ell}\right)^{n_{\ell'}\ i_{\ell' t}}, \quad (21)$$

$$E\left(r_{\ell,t+1}|r_{\ell t}, c_{\ell t}\right) = (1 - \gamma_\ell) r_{\ell,t} + \gamma_\ell c_{\ell t}, \quad (22)$$

where $c_{\ell t} = C_{\ell t}/n_\ell$ and $r_{\ell t} = R_{\ell t}/n_\ell$ refer to per capita infected and recovered by group, respectively, and $\mathbf{i}_t = (i_{1t}, i_{2t}, \ldots, i_{Lt})'$ with $i_{\ell t} = c_{\ell t} - r_{\ell t} = I_{\ell t}/n_\ell$. Given time series data on $\mathbf{c}_t = (c_{1t}, c_{2t}, \ldots, c_{Lt})'$ and $\mathbf{r}_t = (r_{1t}, r_{2t}, \ldots, r_{Lt})'$, the above moment conditions can be used to estimate the structural parameters, γ_ℓ, τ_ℓ and $p_{\ell\ell'} = p_{\ell'\ell}$.

In relating the theory to the data one may need to further aggregate across groups to the population level if group-level data are unavailable or unreliable. It is interesting to note that the multigroup model does not lead to a model for the aggregates, $C_t = \sum_{\ell=1}^{L} C_{\ell t}$ and $I_t = \sum_{\ell=1}^{L} I_{\ell t}$, without strong restrictions. To see this, set $p_{\ell\ell'} = \kappa k_{\ell\ell'}/n_{\ell'}$, where $k_{\ell\ell'}$ is the mean number of contacts per day between individuals in group ℓ and ℓ', and κ is a constant. To preserve the symmetry of contact probabilities the mean contact numbers must satisfy the so-called reciprocity

condition, $n_\ell k_{\ell\ell'} = n_{\ell'} k_{\ell'\ell}$.[10] That is, the total number of contacts that people in group ℓ have with people in group ℓ' must be the same as the number of contacts that people in group ℓ' have with people in group ℓ. In practice n_ℓ is often quite large, with $k_{\ell\ell'}$ relatively small (often less than 30). Then we have

$$\begin{aligned}\ln\left[\left(1-p_{\ell\ell'}+p_{\ell\ell'}e^{-\tau_\ell}\right)^{n_{\ell'}i_{\ell't}}\right] &= n_{\ell'}i_{\ell't}\ln\left[1-p_{\ell\ell'}\left(1-e^{-\tau_\ell}\right)\right] \\ &= -n_{\ell'}i_{\ell't}p_{\ell\ell'}\left(1-e^{-\tau_\ell}\right)+O\left(n_{\ell'}p_{\ell\ell'}^2\right) \\ &= -\kappa\left(1-e^{-\tau_\ell}\right)i_{\ell't}k_{\ell\ell'}+O\left(n_{\ell'}^{-1}\right). \end{aligned} \tag{23}$$

Since $w_\ell = n_\ell/n > 0$, for all ℓ, then n_ℓ rises at the same rate as n, and hence

$$\left(1-p_{\ell\ell'}+p_{\ell\ell'}e^{-\tau_\ell}\right)^{n_{\ell'}\ i_{\ell't}} = \exp\left[-\kappa\left(1-e^{-\tau_\ell}\right)i_{\ell't}k_{\ell\ell'}+O\left(n^{-1}\right)\right].$$

Using the above result in (21) gives

$$E\left(1-c_{\ell,t+1}|\ \mathbf{i}_t\right) = (1-c_{\ell t})\exp\left[-\kappa\left(1-e^{-\tau_\ell}\right)\sum_{\ell'=1}^{L}i_{\ell't}k_{\ell\ell'}+O\left(n^{-1}\right)\right]. \tag{24}$$

It is evident that κ and τ_ℓ are not separably identifiable, and thus we set $\kappa = 1$ hereafter. Let $\beta_{\ell\ell'} = \left(1-e^{-\tau_\ell}\right)k_{\ell\ell'}$. Note that $1-e^{-\tau} = \tau + O\left(\tau^2\right) \approx \tau$ since τ is small. Then we have $\beta_{\ell\ell'} \approx \tau_\ell k_{\ell\ell'}$, and (24) can be rewritten as

$$E\left(1-c_{\ell,t+1}|\ \mathbf{i}_t\right) = (1-c_{\ell t})\exp\left(-\sum_{\ell'=1}^{L}\beta_{\ell\ell'}i_{\ell't}\right)+O\left(n^{-1}\right). \tag{25}$$

Notice that $\sum_{\ell=1}^{L} w_\ell c_\ell = C_t/n = c_t$ and $\sum_{\ell=1}^{L} w_\ell i_\ell = I_t/n = i_t$. If we multiply both sides of (25) by w_ℓ and sum across $\ell = 1, 2, \ldots, L$, we will get

$$\sum_{\ell=1}^{L} w_\ell E\left(1-c_{\ell,t+1}|\ \mathbf{i}_t\right) = \sum_{\ell=1}^{L} w_\ell\left(1-c_{\ell t}\right)\exp\left(-\sum_{\ell'=1}^{L}\beta_{\ell\ell'}i_{\ell't}\right)+O\left(n^{-1}\right),$$

or

$$E\left(1-c_{t+1}|\ \mathbf{i}_t\right) = \sum_{\ell=1}^{L} w_\ell\left(1-c_{\ell t}\right)\exp\left(-\sum_{\ell'=1}^{L}\beta_{\ell\ell'}i_{\ell't}\right)+O\left(n^{-1}\right). \tag{26}$$

[10] See, for example, Willem et al. (2020).

It is now clear that the group moment condition for infected cases, (21), does not aggregate up to the moment conditions in terms of c_t and i_t, unless $\beta_{\ell\ell'}/n_{\ell'}$ is the same across all ℓ and ℓ'. It is also straightforward to see that the group moment condition for recovery, (22), does not aggregate up either unless $\gamma_\ell = \gamma$ for all ℓ.

In the case of a single group, we have $\tau_\ell = \tau$, $k_{\ell\ell'} = k$, and $\beta_{\ell\ell'} = \beta \approx \tau k$, for all ℓ and ℓ'. Then (26) simplifies to

$$E\left(\frac{1-c_{t+1}}{1-c_t}|\ i_t\right) = e^{-\beta i_t} + O\left(n^{-1}\right). \tag{27}$$

Also, if $\gamma_\ell = \gamma$, for all ℓ, the recovery moment condition, (22), becomes

$$E\left(r_{t+1}|r_t, c_t\right) = (1-\gamma)\, r_t + \gamma c_t. \tag{28}$$

Given aggregate data on c_t, i_t and r_t, one can estimate β and γ using the moment conditions (27) and (28), respectively. We shall return to the identification and estimation problem once we have clarified the relationship between our model and the classical SIR model.

4.3 Relation to the multigroup SIR model

The multigroup SIR model given by (8)–(10) is a linearized-deterministic version of the above moment conditions. To see this, using the identity $S_{\ell t} = n_\ell - C_{\ell t}$ and $s_{\ell t} = S_{\ell t}/n_\ell$, (25) can be expressed as

$$E\left(s_{\ell,t+1}|\ \mathbf{i}_t\right) = s_{\ell t} \exp\left(-\sum_{\ell'=1}^{L} \beta_{\ell\ell'} i_{\ell' t}\right) + O\left(n^{-1}\right) \approx s_{\ell t}\left(1 - \sum_{\ell'=1}^{L} \beta_{\ell\ell'} i_{\ell' t}\right) + O\left(n^{-1}\right). \tag{29}$$

Let $\Delta s_{\ell,t+1} = s_{\ell,t+1} - s_{\ell t}$. Then (29) can be rewritten as

$$E\left(\Delta s_{\ell,t+1}|\ \mathbf{i}_t\right) \approx -s_{\ell t} \sum_{\ell'=1}^{L} \beta_{\ell\ell'} i_{\ell' t} + O\left(n^{-1}\right). \tag{30}$$

In comparison, dividing both sides of (8) in the multigroup SIR model gives

$$\Delta s_{\ell,t+1} = -s_{\ell t} \sum_{\ell'=1}^{L} \beta_{\ell\ell'} i_{\ell' t}. \tag{31}$$

To exactly match the deterministic expression of $s_{\ell t}$ given by (31) with the stochastic process given by (30), we can introduce either an additive or a multiplicative random error to the right-hand side of (31). To ensure that $s_{\ell t}$ is non-negative for all t, a multiplicative error with mean unity would be a more reasonable choice.

Turning to the recovery process. The aggregate recovery governed by (20) matches with the deterministic recovery equation, (10), of the SIR model under a geometric recovery process. Finally, since $I_{\ell t} = n_\ell - R_{\ell t} + S_{\ell t}$, the active cases of our model also match with the infected equation, (9), of the SIR model.

5 Basic and effective reproduction numbers

In this section we consider the calibration of our model to a given basic reproduction number assuming no intervention, and derive the effective reproduction numbers in terms of mean contact patterns, exposure intensities, and the recovery rate. We also highlight the difficulty in identifying the contact patterns from the exposure rates in single and multigroup contexts.

5.1 Basic reproduction number

We calibrate the parameters of our model so that at the start of the disease outbreak (the initial state) the model yields the basic reproduction number, denoted by $\mathcal{R}_0$, formally defined as "*the average number of secondary cases produced by one infected individual during the infected individual's entire infectious period assuming a fully susceptible population*" (Del Valle, Hyman, and Chitnis, 2013). By construction, $\mathcal{R}_0$ measures the ability of an infectious disease spreading in the absence of any interventions. Infection spreads if $\mathcal{R}_0 > 1$ and abates if $\mathcal{R}_0 < 1$.

Suppose that in day 1, the equivalent of one individual becomes infected. To capture the different contact and exposure intensities of the groups, we assume that a fraction $w_\ell = n_\ell/n$ of each group ℓ becomes infected. That is, in day 1, $R_{\ell 1} = 0$, $I_{\ell 1} = C_{\ell 1} = w_\ell$ for $\ell = 1, 2, \ldots, L$. In

day 2, using (19) we obtain ($\mathbf{w} = (w_1, w_2, \ldots, w_L)'$)

$$E\left(C_{\ell 2}|\ \mathbf{w}\right) = n_\ell \left[1 - \prod_{\ell'=1}^{L} \left(1 - p_{\ell\ell'} + p_{\ell\ell'} e^{-\tau_\ell}\right)^{w_{\ell'}}\right], \tag{32}$$

for all ℓ. To simplify the exposition, suppose that $\gamma_\ell = \gamma$, for all ℓ. Then the average infection duration is $1/\gamma$. Assume further that the individual remains infected over the infectious period, $1/\gamma$. According to the definition of $\mathcal{R}_0$, we need to match $\sum_{\ell=1}^{L} E\left(C_{\ell 2}|\ \mathbf{w}\right)$ to $\gamma\mathcal{R}_0$, namely set

$$\gamma\mathcal{R}_0 = n - \sum_{\ell=1}^{L} n_\ell \prod_{\ell'=1}^{L} \left(1 - p_{\ell\ell'} + p_{\ell\ell'} e^{-\tau_\ell}\right)^{w_{\ell'}}. \tag{33}$$

This is an exact multigroup expression for $\mathcal{R}_0$ and it plays a critical role in identification and the calibration exercises to follow.

To see how the expression in (33) relates to the well known expression $\mathcal{R}_0 = \beta/\gamma$, consider the case of a single group with $p = k/(n-1) \approx k/n$ since n is large. Then the expression in (33) reduces to

$$\gamma\mathcal{R}_0 = n\left[1 - \left(1 - p + pe^{-\tau}\right)\right] = np(1 - e^{-\tau}) \approx \tau k, \tag{34}$$

where the last result follows by $1 - e^{-\tau} = \tau + O\left(\tau^2\right)$, and τ being small. Hence the model can be calibrated to any choice of $\mathcal{R}_0$ and γ by setting the average number of contacts, k, and/or the exposure intensity parameter, τ. It is clear that τ and k are not separately identified—only their product is identified. In addition, we would obtain the classical result $\gamma\mathcal{R}_0 = \beta$ in SIR models if we set $\beta = np(1 - e^{-\tau}) \approx \tau k$.

Returning to the multigroup case, expression (34) continues to apply if the population is homogeneous in the sense that $p_{\ell\ell'} = p$, $\tau_\ell = \tau$, for all ℓ and ℓ'. But in the more realistic case of group heterogeneity we can use (33) to calibrate τ_ℓ and/or $p_{\ell\ell'}$ for given choices of $\mathcal{R}_0$ and γ. Since we have assumed that n_ℓ is large and L is fixed, (33) can be further simplified with a linear approximation derived as follows. Let $A_{n,\ell\ell'} = \left(1 - p_{\ell\ell'} + p_{\ell\ell'} e^{-\tau_\ell}\right)^{w_{\ell'}}$, and use a similar argument

as in (23) to obtain (recall that $p_{\ell\ell'} = O(n^{-1})$)

$$\begin{aligned}\ln A_{n,\ell\ell'} &= w_{\ell'} \ln\left[1 - p_{\ell\ell'}\left(1 - e^{-\tau_\ell}\right)\right] = -w_{\ell'} p_{\ell\ell'}\left(1 - e^{-\tau_\ell}\right) + O\left(p_{\ell\ell'}^2\right) \\ &\approx -\tau_\ell w_{\ell'} p_{\ell\ell'} + O\left(n^{-2}\right).\end{aligned}$$

Then $A_{n,\ell\ell'} = \exp\left(-\tau_\ell w_{\ell'} p_{\ell\ell'}\right) + O\left(n^{-2}\right)$. Using this in (33) gives

$$\begin{aligned}\gamma\mathcal{R}_0 &= n - \sum_{\ell=1}^{L} n_\ell \left\{\exp\left(-\tau_\ell \sum_{\ell'=1}^{L} w_{\ell'} p_{\ell\ell'}\right) + O\left(n^{-2}\right)\right\} \\ &= \sum_{\ell=1}^{L} n_\ell \tau_\ell \sum_{\ell'=1}^{L} w_{\ell'} p_{\ell\ell'} + O\left(n^{-1}\right) \\ &= n \sum_{\ell=1}^{L}\sum_{\ell'=1}^{L} w_\ell w_{\ell'}\left(\tau_\ell p_{\ell\ell'}\right) + O\left(n^{-1}\right). \end{aligned} \tag{35}$$

As before setting $p_{\ell\ell'} = k_{\ell\ell'}/n_{\ell'}$ the above expression can be written equivalently as

$$\gamma\mathcal{R}_0 = \sum_{\ell=1}^{L} w_\ell \beta_\ell + O\left(n^{-1}\right), \tag{36}$$

where β_ℓ is the group-specific transmission rate defined by

$$\beta_\ell = \sum_{\ell'=1}^{L} \tau_\ell k_{\ell\ell'}. \tag{37}$$

Similar to the case of a single group, equation (35) implies that τ_ℓ and $p_{\ell\ell'}$ are not separately identified; only their products are identified (or equivalently, $\beta_{\ell\ell'} \approx \tau_\ell k_{\ell\ell'}$ are identified). To see this more formally, consider the simple case of two groups ($L = 2$). Then for sufficiently large n, using (35) with $L = 2$ we have

$$\begin{aligned}\gamma\mathcal{R}_0 &\approx n w_1\left(w_1\tau_1 p_{11} + w_2\tau_1 p_{12}\right) + n w_2\left(w_1\tau_2 p_{21} + w_2\tau_2 p_{22}\right) \\ &= n w_1^2\left(\tau_1 p_{11}\right) + n w_1 w_2\left(\tau_1 p_{12} + \tau_2 p_{21}\right) + n w_2^2\left(\tau_2 p_{22}\right) \\ &= n w_1^2\left(\tau_1 p_{11}\right) + n w_1 w_2\left(\tau_1 + \tau_2\right) p_{12} + n w_2^2\left(\tau_2 p_{22}\right), \end{aligned} \tag{38}$$

where the last line follows by the symmetry of contact probabilities: $p_{\ell\ell'} = p_{\ell'\ell}$. It is clear from (38) that only $\tau_1 p_{11}$, $(\tau_1 + \tau_2)\, p_{12}$, and $\tau_2 p_{22}$ can be identified given w_1, w_2, n and γ. More generally,

for finite $L \geq 2$, $\tau_\ell p_{\ell\ell'}$ are identified for any ℓ and $\ell' = 1, 2, \ldots, L$.

5.2 Effective reproduction numbers and mitigation policies

In reality, the average number of secondary cases will vary over time as a result of decline in the number of susceptible individuals (due to immunity or death) and/or changes in behavior (due to mitigation strategies such as social distancing, quarantine measures, travel restrictions and wearing of facemasks). The effective reproduction number, which we denote by $\mathcal{R}_{et}$,[11] is the expected number of secondary cases produced by one infected individual in a population that includes both susceptible and non-susceptible individuals at time t. In a multigroup setting we represent "one infected individual" by the vector of population proportions, $\mathbf{w} = (w_1, w_2, \ldots, w_L)'$. The evolution of $\mathcal{R}_{et}$ is determined by the remaining number of susceptibles by groups, $S_{\ell t} = n_\ell - C_{\ell t}$, for $\ell = 1, 2, \ldots, L$. Formally, $\mathcal{R}_{et}$ is defined by

$$\gamma \mathcal{R}_{et} = \sum_{\ell=1}^{L} E\left(C_{\ell,t+1} - C_{\ell t} | \ \mathbf{I}_t = \mathbf{w}\right). \tag{39}$$

In the absence of any interventions, using (19) we have

$$\gamma \mathcal{R}_{et} = \sum_{\ell=1}^{L} \left(n_\ell - C_{\ell t}\right) \left[1 - \prod_{\ell'=1}^{L} \left(1 - p_{\ell\ell'} + p_{\ell\ell'} e^{-\tau_\ell}\right)^{w_{\ell'}}\right]. \tag{40}$$

Recalling that $\left(1 - p_{\ell\ell'} + p_{\ell\ell'} e^{-\tau_\ell}\right)^{w_{\ell'}} = \exp\left(-\tau_\ell w_{\ell'} p_{\ell\ell'}\right) + O\left(n^{-2}\right)$, then for n sufficiently large we have the following approximate expression for $\mathcal{R}_{et}$:

$$\gamma \mathcal{R}_{et} = \sum_{\ell=1}^{L} S_{\ell t} \left(\sum_{\ell'=1}^{L} \tau_\ell w_{\ell'} p_{\ell\ell'}\right) + O\left(n^{-1}\right),$$

Setting $p_{\ell\ell'} = k_{\ell\ell'}/n_{\ell'}$ we can alternatively write $\gamma \mathcal{R}_{et}$ as (recall that $w_{\ell'} = n_{\ell'}/n$ and $s_{\ell t} = S_{\ell t}/n_\ell$)

$$\gamma \mathcal{R}_{et} = \sum_{\ell=1}^{L} w_\ell \beta_\ell s_{\ell t} + O\left(n^{-1}\right), \tag{41}$$

where β_ℓ is already defined by (37).

In the case of a single group or when $\beta_\ell = \beta$ is homogeneous across groups, the above expression

[11] We use this notation in order to clearly distinguish the effective reproduction number from the number of removed cases, R_t.

simplifies to $\gamma \mathcal{R}_{et} = \beta \left(\sum_{\ell=1}^{L} w_\ell s_{\ell t} \right) = \beta s_t$, which can be written equivalently as

$$\mathcal{R}_{et} = (1 - c_t)\mathcal{R}_0. \tag{42}$$

In the absence of any interventions $\mathcal{R}_{et}$ declines as c_t rises, and $\mathcal{R}_{et}$ falls below 1 when $c_t > (\mathcal{R}_0 - 1)/\mathcal{R}_0$. The value $(\mathcal{R}_0 - 1)/\mathcal{R}_0$ is often referred to as the herd immunity threshold. For the multigroup case, using (36) and (41), the condition for herd immunity is more complicated and is given by (for n sufficiently large)

$$\frac{\sum_{\ell=1}^{L} w_\ell \beta_\ell s_{\ell t}}{\gamma} = \left[\frac{\sum_{\ell=1}^{L} w_\ell \beta_\ell \left(1 - c_{\ell t}\right)}{\sum_{\ell=1}^{L} w_\ell \beta_\ell} \right] \mathcal{R}_0 < 1,$$

and the herd immunity threshold becomes

$$\frac{\sum_{\ell=1}^{L} w_\ell \beta_\ell c_{\ell t}}{\sum_{\ell=1}^{L} w_\ell \beta_\ell} > \frac{\mathcal{R}_0 - 1}{\mathcal{R}_0}.$$

This formula clearly shows that for herd immunity to apply, the group-specific infection rate, $c_{\ell t}$, must be sufficiently large – shielding one group requires higher infection rates in other groups with larger population weights. To see this, let us consider a simple example of two groups ($L = 2$) with a homogeneous transmission rate across the two groups ($\beta_1 = \beta_2 = \beta$). Suppose that policy makers want to shield Group 1, which may comprise elderly people, from infection. In the extreme case where all individuals in Group 1 are protected, namely, $c_{1t} = 0$, then herd immunity requires $c_{2t} > (\mathcal{R}_0 - 1)/(\mathcal{R}_0 w_2)$, which is higher than the threshold value of $(\mathcal{R}_0 - 1)/\mathcal{R}_0$ where the population groups are treated symmetrically.

Social intervention might be necessary if the herd immunity threshold is too high and could lead to significant hospitalization and deaths. In such cases intervention becomes necessary to reduce the transmission rates β_ℓ, thus introducing independent policy-induced reductions in the transmission rates. In the presence of social policy interventions the effective reproduction number for the multigroup can be written as

$$\gamma \mathcal{R}_{et} = \sum_{\ell=1}^{L} w_\ell \beta_{\ell t} s_{\ell t} + O\left(n^{-1}\right). \tag{43}$$

where (using (37))

$$\beta_{\ell t} = \sum_{\ell'=1}^{L} \tau_{\ell t} k_{\ell \ell', t}.$$

Reductions in $\beta_{\ell t}$ can come about either by reducing the average number of contacts within and across groups, $k_{\ell \ell', t}$, or by reducing the group-specific exposure intensity parameter, $\tau_{\ell t}$, or both. Since only the product of $\tau_{\ell t}$ and $k_{\ell \ell', t}$ is identified, in our simulations we fix the contact patterns and calibrate the desired value of $\beta_{\ell t}$ by setting the value of $\tau_{\ell t}$ for each ℓ to achieve a desired $\mathcal{R}$ number. Of course, one would obtain equivalent results if the average number of contacts is assumed to be time-varying and the exposure intensity parameter is assumed constant. In the case of a single group or when $\beta_{\ell t} = \beta_t$ for all ℓ, we have

$$\mathcal{R}_{et} = (1 - c_t)\frac{\beta_t}{\gamma}, \tag{44}$$

where $(1 - c_t)$ is the herding component. It is also worth bearing in mind that at the outset of epidemic outbreaks the value of c_t is close to zero which ensures that $\mathcal{R}_{e0} = \beta_0/\gamma = \mathcal{R}_0$.

6 Simulated properties of the model

We are now in a position to examine the properties of the model by simulations. We first present simulation results for a fixed transmission rate, β, (assuming no intervention) using the single and multigroup models. We then consider simulation outcomes under two scenarios with social interventions such that the transmission rate, β_t, is linearly declining and W-shaped, respectively.

6.1 Simulations with a fixed transmission rate

Although it is difficult to obtain an analytical solution to the individual based stochastic epidemic model, we can study its properties by simulations. We start with the baseline case of a single group ($L = 1$), with no interventions, so that the transmission rate is a constant. In light of the recent studies on the value of $\mathcal{R}_0$ for Covid-19 we set $\mathcal{R}_0 = 3$. A summary of published estimates of $\mathcal{R}_0$ is provided in Table 1 of D'Arienzo and Coniglio (2020). For the recovery rate, in view of

the World Health Organization guidelines of two weeks self-isolation we set $\gamma = 1/14$.[12] It follows that $\beta = \gamma\mathcal{R}_0 = 3/14$. Recall that $\beta = \tau k$ and, as has been shown in Section 5, τ and k are not separately identified. We set the average number of contacts to $k = 10$ based on the literature on social contacts in the pre-Covid period that we have reviewed in Section 2, and then set the exposure intensity parameter, τ, by $\tau = \beta/k = \gamma\mathcal{R}_0/k$.

For each replication, the simulation begins with 1/1000 of the population randomly infected in day 1, that is, $c_1^{(b)} = i_1^{(b)} = 0.001$, and $r_1^{(b)} = 0$, where b denote the b^{th} replication, for $b = 1, 2, \ldots, B$.[13] Then from day 2 onwards, the infection and recovery processes follow (11) and (14), respectively, with $L = 1$. After obtaining $x_{i,t}^{(b)}$, $y_{i,t}^{(b)}$ and $z_{i,t}^{(b)}$, we compute the aggregates, $C_t^{(b)} = \sum_{i=1}^n x_{i,t}^{(b)}$, $R_t^{(b)} = \sum_{i=1}^n y_{i,t}^{(b)}$ and $I_t^{(b)} = \sum_{i=1}^n z_{i,t}^{(b)}$. We consider $B = 1,000$ replications and set the population size to $n = 10,000$. We also tried larger population sizes but, as will be seen below, the interquartile range of the simulated infected and active cases is very tight when $n = 10,000$. Some simulation results for $n = 50,000$ and $n = 100,000$ are provided in Figure S.1 of the Online Supplement.

The only remaining task is to determine the topology of the contact network which, in the case of a single group, can be denoted by $\mathbf{D}^{(b)}(t) = \left(d_{ij}^{(b)}(t)\right)$. Note that the contact network randomly changes every day (and also across replications). This feature captures the random nature of many encounters an individual has on a daily basis. We consider two widely used random networks: Erdős-Rényi and power law (also known as scale-free) random networks. In an Erdős-Rényi random graph (simply referred to as "the" random graph), each pair of the nodes (or individuals) are connected at random with a uniform probability $p = k/(n-1) \approx k/n$, where k is the mean degree of the network (or mean number of contacts per individual).[14] Note that in the limit of large n (with k fixed), the Erdős-Rényi random network has a Poisson degree distribution, which may depart from real-world contact networks in which a small number of individuals (such

[12] Similar guidelines issued by U.S. and U.K. can be found at `https://www.cdc.gov/coronavirus/2019-ncov/if-you-are-sick/quarantine.html` and `https://www.nhs.uk/conditions/coronavirus-covid-19/self-isolation-and-treatment/how-long-to-self-isolate/`, respectively.

[13] We find that there will not be outbreaks in many replications if the simulation begins with less than 1/1000 of the population initially infected.

[14] The degree of a node in a network is the number of connections it has (or number of edges attached to it).

as school-aged children, medical professionals, delivery drivers and sales workers) may have a relatively high number of daily contacts. In other words, the degree distribution of the contact networks may be heavy-tailed (right-skewed). The power law random network is a popular choice to model this phenomenon. In a (truncated) power law graph, the degree distribution follows the power-law distribution:

$$p_x = Cx^{-\alpha}, \quad x = k_{\min}, k_{\min}+1, \ldots, k_{\max}, \tag{45}$$

where p_x is the fraction of nodes in the graph with degree x, $k_{\min}$ ($k_{\max}$) is the minimum (maximum) degree, $\alpha > 1$ is a constant known as the power law exponent, and C is a normalization constant such that $\sum_{k_{\min}}^{k_{\max}} p_x = 1$. We consider $k_{\min} = 5$ and $k_{\max} = 50$ in the simulations. The value of α is set so that the mean degree is equal to 10. We provide details on the generation of the Erdős-Rényi and power law networks in Section S2 of the Online Supplement.

Figure 1 presents the simulation results using the power law contact network. It displays in fan chart style with the 10^{th}, 25^{th}, 50^{th}, 75^{th} and 90^{th} percentiles of the proportion of infected, $c_t^{(b)} = C_t^{(b)}/n$, and the proportion of active cases, $i_t^{(b)} = I_t^{(b)}/n$, over $1,000$ replications. The mean values are very close to the median and hence not shown. We see that the proportion of infected starts to increase rapidly around 40 days since the outbreak, and then begins to level off about 90 days after the start of the outbreak. The maximum proportion of infected averaged across replications, i.e., $c_{\max} = B^{-1}\sum_{b=1}^{B} \max_t \left(c_t^{(b)}\right)$, eventually peaks at 93.8 percent, which is markedly higher than the peak value of 2/3 obtained for deterministic SIR models with the same basic reproduction number. The proportion of active cases is slightly right-skewed and reaches maximum, $i_{\max} = B^{-1}\sum_{b=1}^{B} \max_t \left(i_t^{(b)}\right) = 0.298$, about 59 days since the outbreak. The simulation results using the Erdős-Rényi random network are very similar to those obtained using the power law network with the same mean degree. (See Figure S.3 of the Online Supplement.) Therefore, in what follows we will focus on the power law network.

We now turn to the multigroup case. For illustrative purposes, we consider dividing the population into $L = 3$ age groups: $[0, 15)$, $[15, 65)$ and 65+ years old. We calibrate the model to

Figure 1: Simulated number of infected and active cases using a single group model with $\mathcal{R}_0 = 3$

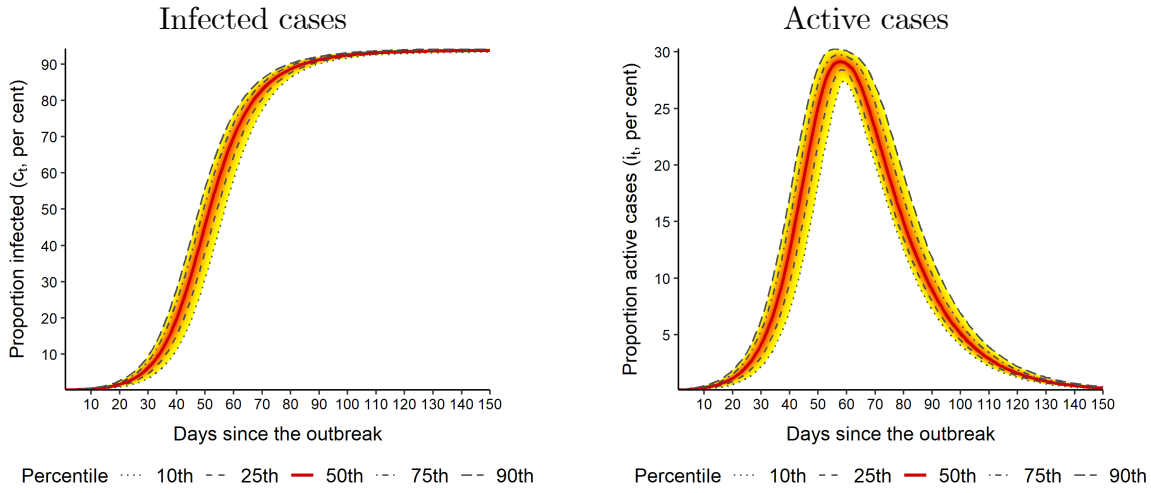

Notes: The simulation uses the power law network with mean contact number $k = 10$ and begins with 1/1000 of the population randomly infected in day 1. The exposure intensity parameter is set to $\tau = \gamma\mathcal{R}_0/k$, with $\mathcal{R}_0 = 3$ and recovery rate $\gamma = 1/14$. Population size is $n = 10,000$. Number of replications is $1,000$.

the contact matrix reported by Mossong et al. (2008) for Germany, which is given by

$$K = (k_{\ell\ell'}) = \begin{pmatrix} 3.396 & 4.109 & 0.425 \\ 0.879 & 6.812 & 0.641 \\ 0.351 & 2.471 & 1.671 \end{pmatrix}. \tag{46}$$

The associated population shares are $\mathbf{w} = (w_1, w_2, w_3)' = (0.145, 0.679, 0.176)'$.[15] Recall that τ_ℓ and $p_{\ell\ell'} = k_{\ell\ell'}/n_{\ell'}$ are not separately identified.[16] To capture the fact that older people are more likely to be infected, we follow the study by Zhang et al. (2020a) who estimate that the odds ratios for a contact of age group 1 and 3 to be infected relative to age group 2 are 0.34 and 1.47, respectively. Accordingly, we set $\boldsymbol{\tau} = (\tau_1, \tau_2, \tau_3)' = \tau_2 (0.34, 1, 1.47)'$, and then calibrate τ_2 such that

$$\gamma\mathcal{R}_0 = n \sum_{\ell=1}^{L} \sum_{\ell'=1}^{L} w_\ell w_{\ell'} (\tau_\ell p_{\ell\ell'}),$$

As in the case of a single group, we set $\mathcal{R}_0 = 3$ and $\gamma = 1/14$. For each replication the simulation

[15] These data can be easily retrieved by the Social Contact Rates (SOCRATES) Data Tool at `https://lwillem.shinyapps.io/socrates_rshiny/`.

[16] See Section S2 of the Online Supplement for the generation of networks with the multigroup structure.

begins with 1/1000 of total population ($n = 10,000$) randomly infected in day $t = 1$, and then from $t = 2$ onwards, the infection and recovery processes follow (11) and (14), for $\ell = 1, 2, 3$. We compute $c_{\ell t}^{(b)} = C_{\ell t}^{(b)}/n_\ell$ and $i_{\ell t}^{(b)} = I_{\ell t}^{(b)}/n_\ell$ for each group, and the associated aggregate measures $c_t^{(b)} = \sum_{\ell=1}^{L} w_\ell c_{\ell t}^{(b)}$ and $i_t^{(b)} = \sum_{\ell=1}^{L} w_\ell i_{\ell t}^{(b)}$. As before, the number of replications is set to $B = 1,000$.

Figure 2 displays the simulation results for the three groups separately. As before, the fan charts depict the 10^{th} percentile through the 90^{th} percentile of $c_{\ell t}^{(b)}$ and $i_{\ell t}^{(b)}$; the mean and median values are quite close. Among the young people in Group 1, the proportion of infected peaks at 59.1 percent, compared to the maximum proportion of infected equaling 95.8 and 91.9 percents for Groups 2 and 3, respectively. For the proportion of new cases, Group 1 peaks at 16.2 percent, a level much lower than 32.2 percent for Group 2 and 29.6 percent for Group 3, respectively. It takes 64, 55, and 57 days, respectively, for the 3 groups to reach their peak proportion of new cases. Of course, these outcomes depend on our specification of the contact matrix and the exposure intensity parameters. This exercise aims to demonstrate the simulations with the multigroup model, rather than produce results that are close to the real data.

It is also of interest to compare the aggregates obtained using the multigroup model with those from the single group model. Figure 3 compares the median values of $c_t^{(b)}$ and $i_t^{(b)}$ over $1,000$ replications. What stands out is the similarity of the epidemic curves whether they are obtained by multigroup or the single group model.[17] This is not surprising because the simulations were performed with the same fixed $\beta = \gamma \mathcal{R}_0$. The heterogeneity in τ_ℓ and $p_{\ell\ell'}$ affects the epidemic curves for each group, but do not seem to impact the aggregates. This is interesting and suggests that an aggregate analysis might be justified if the primary focus is on the spread of the infection across the population as a whole rather than on particular age/type groups.

[17] We also obtain similar results when we carry out simulations using 6 and 8 groups instead of 3 groups.

Figure 2: Simulated number of infected and active cases using a multigroup model with $\mathcal{R}_0 = 3$

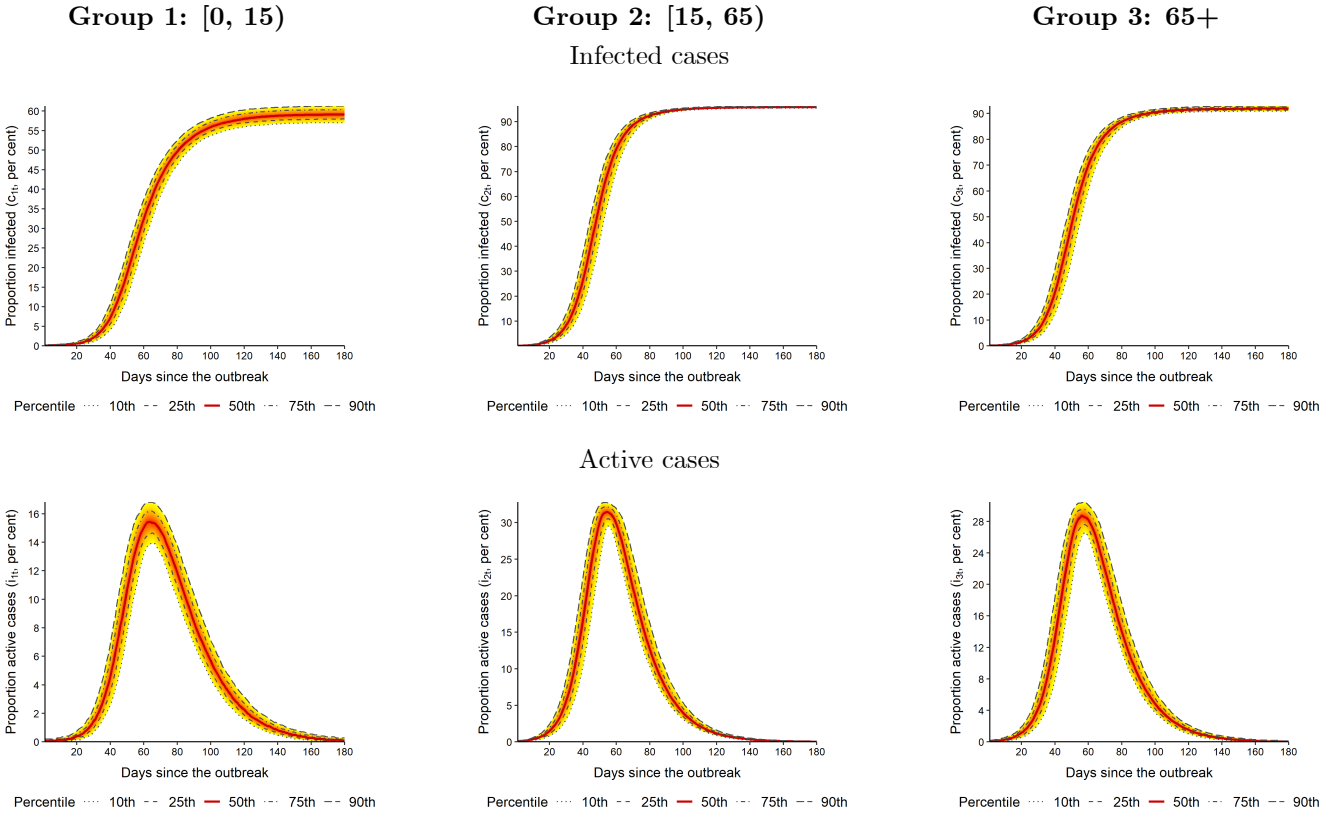

Notes: We set 1/1000 of the population randomly infected in day 1. Recovery rate is $\gamma = 1/14$. The contact matrix is given by (46). Population size is $n = 10,000$, with population shares $\mathbf{w} = (0.145, 0.679, 0.176)'$. Number of replications is $1,000$.

6.2 Simulations with linearly declining and W-shaped transmission rates

In reality, the transmission rate varies over time both due to voluntary and mandated social distancing and other mitigation measures, as well as changes in the share of susceptible population as the epidemic spreads. But at the early stage of the epidemic the main driver of the transmission rate is behavioral. Here we consider two scenarios—linearly declining β_t and W-shaped β_t—that are representative of transmission rates we observe as a result of different mitigation policies. We focus on the case of a single group, but note that similar simulations can be conducted for the multigroup model.

In the case of linearly declining β_t, we let β_t decrease linearly from $\beta_0 = \mathcal{R}_0\gamma = 3/14$ at

Figure 3: Median number of infected and active cases under single- and multi-group models with $\mathcal{R}_0 = 3$

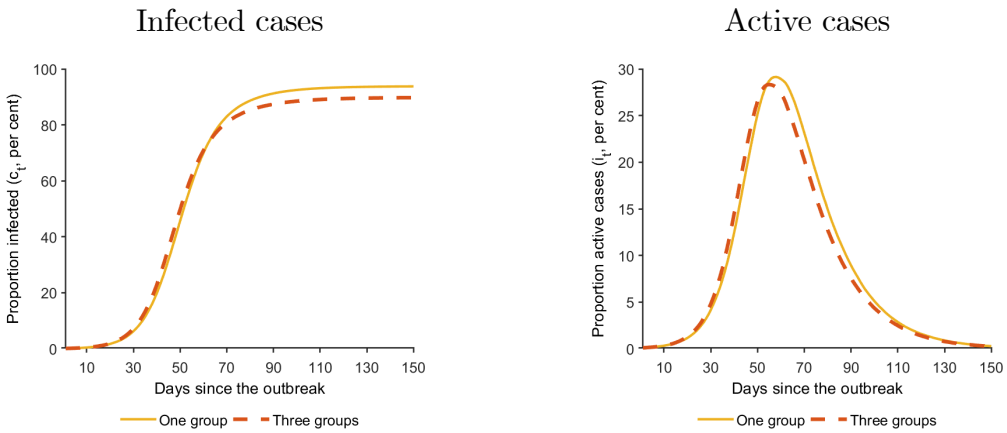

Notes: Median values of $c_t^{(b)}$ and $i_t^{(b)}$ over replications $b = 1, 2, \ldots, 1,000$ are displayed. Recovery rate is $\gamma = 1/14$. Population size is $n = 10,000$. In the case of a single group, the power law network with mean contact number $k = 10$ was used. In the case of the multigroup model, the contact matrix is given by (46) and population shares are $\mathbf{w} = (0.145, 0.679, 0.176)'$.

the rate of 0.0023 per day during the first 80 days since the outbreak and then remain constant thereafter. In the case of W-shaped β_t, we set β_t to fall linearly from 3/14 at the daily rate of 0.0037 in the first 7 weeks, stay constant for another 2 weeks, then rise linearly at the rate of 0.0038 during the $10^{th} - 12^{th}$ weeks, fall linearly at the rate of 0.0031 during the $13^{th} - 18^{th}$ weeks, and finally remain constant until the epidemic is over. We carry out simulations using the power law network assuming a single group. Since τ_t and k_t are not separately identified, as have been shown in Section 5, in simulations we fix $k = 10$ and set $\tau_t = \beta_t/k$. As before, we set $\gamma = 1/14$ and suppose that 1/1000 of population is randomly infected in day 1.

Figure 4 presents the simulation results with linearly declining and W-shaped β_t, in comparison with the results without intervention (with a fixed β), over 180 days since the outbreak. The figure also displays the time profile of β_t (scaled by $1/\gamma$) and the median of $\mathcal{R}_{et}^{(b)} = (1 - c_t^{(b)})\beta_t/\gamma$ over $1,000$ replications. With linearly declining β_t, we find that the maximum proportion of infected was brought down from 93.8 percent under no intervention to 18.8 percent; and the maximum proportion of active cases was significantly reduced from 29.8 percent under no intervention to 4.64 percent. With W-shaped β_t, we obtain two peaks in the active cases – this shows that our model

Figure 4: Simulated number of infected and active cases using a single group model under linearly declining and W-shaped transmission rates

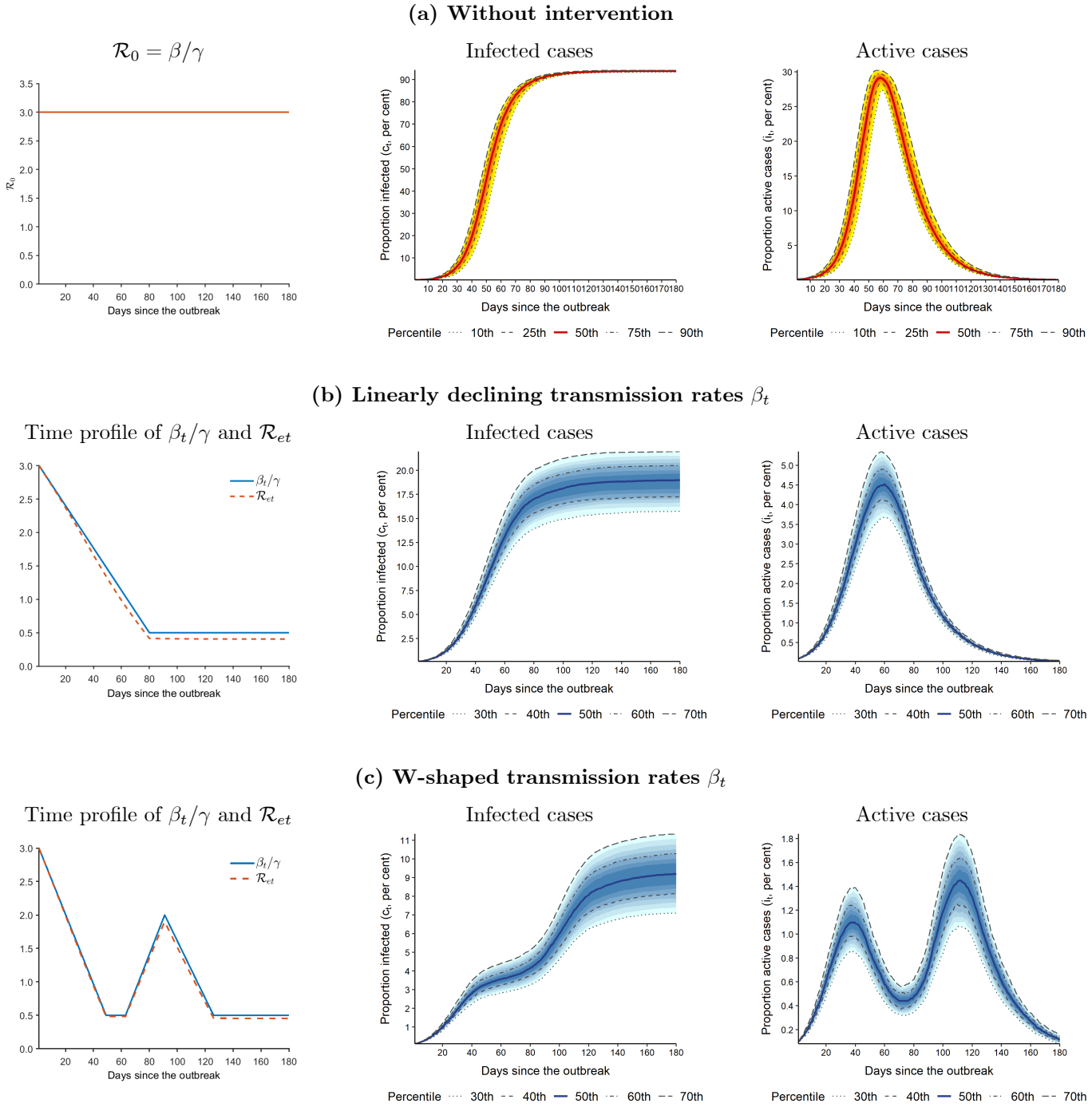

Notes: We set 1/1000 of the population randomly infected in day 1 and use the power law network with mean contact number $k = 10$. Recovery rate is $\gamma = 1/14$. The exposure intensity parameter is $\tau_t = \beta_t/k$. Population size is $n = 10,000$. The median of $\mathcal{R}_{et}^{(b)} = (1 - c_t^{(b)})\beta_t/\gamma$ over $1,000$ replications is displayed together with β_t/γ in the first column.

Figure 5: Median number of infected and active cases using a single group model under linearly declining and W-shaped transmission rates

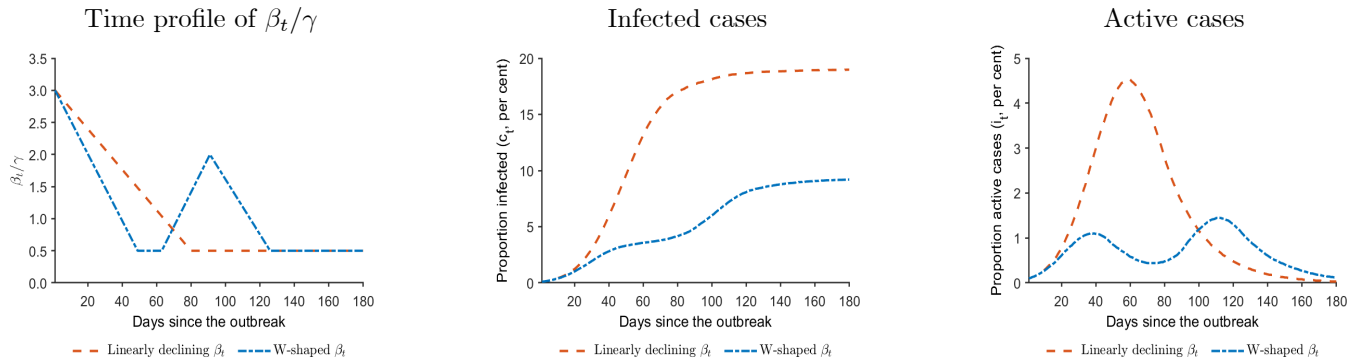

Notes: The simulation uses the power law network with mean contact number $k = 10$ and begins with 1/1000 of the population randomly infected in day 1. Recovery rate is $\gamma = 1/14$. The exposure intensity parameter is $\tau_t = \beta_t/k$. Population size is $n = 10,000$. Number of replications is $1,000$.

is able to produce results that mimic the rebound in Covid-19 cases many countries are currently experiencing. After 180 days the proportion of infected cases accumulates to 9.35 percent, a level much lower than that in the case of no intervention. As expected the difference between β_t/γ and $\mathcal{R}_{et}$ is negligible at the beginning of the outbreak as c_t is very small; β_t/γ becomes higher than $\mathcal{R}_{et}$ as c_t grows. To further compare the scenarios of linearly declining β_t and W-shaped β_t, we plot the median infected and active cases over $1,000$ replications in Figure 5. It is clear that the maximum infected and active cases are much higher with the linearly declining β_t than with the W-shaped β_t. Even though there is a surge in β_t in the latter scenario, this comparison highlights the importance of lowering β_t sooner rather than later.

7 Estimation of transmission rates

The previous section investigates the properties of the model assuming the transmission rates are given. We now turn to detailing how to estimate the transmission rate using data on infected cases. We first derive the method of moments estimation of the transmission rate, present the finite sample properties of the estimators using Monte Carlo techniques, and then show that the estimates are robust to considerable under-reporting of infected cases.

7.1 Estimation without measurement errors

Let us first consider the case of a single group, and recall that the moment condition for this case is given by (27), which is replicated here for convenience

$$E\left(\frac{1-c_{t+1}}{1-c_t}|\ i_t\right)=e^{-\beta i_t}+O\left(n^{-1}\right). \tag{47}$$

We can estimate the transmission rate, β, using (47) by nonlinear least squares (NLS) given time series data on $\{c_t, i_t\}$. The recovery rate, γ, can be estimated using the recovery equation, (22): $E\left(r_{t+1}|r_t, c_t\right) = (1-\gamma)\, r_t + \gamma c_t$. We will discuss the estimation of γ in the next section, but note that in reality, r_t is often not recorded in a timely manner and γ is estimated from the hospitalization data. In the absence of any interventions (voluntary or mandated), $\beta = \gamma\mathcal{R}_0$, where as before $\mathcal{R}_0$ is the basic reproduction number. Then it follows that $\mathcal{R}_0$ can be estimated by $\hat{\mathcal{R}}_0 = \hat{\beta}/\gamma$, where $\hat{\beta}$ is the NLS estimate of β using (47).

To examine the finite sample performance of $\hat{\beta}$, we estimate β using simulated data generated from the stochastic SIR model on a power law network with mean contact $k = 10$ and assuming 1/1000 of the population is randomly infected on day 1. The true value of the transmission rate is set to $\beta = 3/14$, which corresponds to the case where $\mathcal{R}_0 = 3$ and $\gamma = 1/14$.[18] We consider population sizes $n = 5,000$, $10,000$, $50,000$ and $100,000$, and set the the number of replications to $B = 1,000$. To alleviate noise induced by zero and near zero observations at the start and the final stages of the epidemic, estimation of β is carried out over samples with $i_t^{(b)} \geq 0.01$, for the b^{th} replication, $b = 1, 2, \ldots, B$.

Since the value of β is quite small, we present the estimation results in terms of $\hat{\mathcal{R}}_0 = \hat{\beta}/\gamma$. Table 1 summarizes the bias and root mean square error (RMSE) of $\hat{\mathcal{R}}_0$ under different population sizes, where the bias is computed as $B^{-1}\sum_{b=1}^{B}\left(\hat{\mathcal{R}}_0^{(b)} - \mathcal{R}_0\right)$, and the RMSE is computed by $\sqrt{B^{-1}\sum_{b=1}^{B}\left(\hat{\mathcal{R}}_0^{(b)} - \mathcal{R}_0\right)^2}$, where $\hat{\mathcal{R}}_0^{(b)} = \hat{\beta}^{(b)}/\gamma$ and $\hat{\beta}^{(b)}$ is the estimate of β in the b^{th} simulated sample. As can be seen from Table 1, although $\hat{\mathcal{R}}_0$ slightly underestimates $\mathcal{R}_0$, its bias and RMSE are quite small in all experiments. The RMSE declines as the population size n increases, but

[18] For the rationale behind setting $\gamma = 1/14$, see Footnote 12.

Table 1: Finite sample properties of the moment estimator of $\mathcal{R}_0$

		Full	Sub-samples		
Population		Sample	Start	Middle	End
$n = 5,000$	Bias	-0.040	-0.046	-0.039	-0.023
	RMSE	0.068	0.079	0.086	0.320
$n = 10,000$	Bias	-0.037	-0.039	-0.038	-0.010
	RMSE	0.054	0.059	0.067	0.220
$n = 50,000$	Bias	-0.033	-0.032	-0.035	-0.012
	RMSE	0.038	0.038	0.043	0.100
$n = 100,000$	Bias	-0.033	-0.032	-0.035	-0.008
	RMSE	0.035	0.035	0.039	0.073
T		110	37	36	38

Notes: The true value of $\mathcal{R}_0$ is set to β/γ, where $\beta = 3/14$ and $\gamma = 1/14$ so that $\mathcal{R}_0 = 3$. We fix γ and estimate β using (47). Each sub-sample is about 1/3 of the full time series sample size. The time series sample sizes averaged across replications are reported in the last row. Number of replications is $B = 1,000$.

even with $n = 5,000$, $\mathcal{R}_0$ can be estimated reasonably well. In the absence of any interventions we would expect to obtain the same estimate of $\mathcal{R}_0$ irrespective of what sub-sample we consider. To illustrate the robustness of $\hat{\mathcal{R}}_0$ to the choice of the sub-sample, we estimated $\mathcal{R}_0$ over three non-overlapping sub-samples, each around one third of the full sample, at the start, in the middle, and at the end of the epidemic. The results show that $\mathcal{R}_0$ can be estimated fairly well over all of the three sub-samples.

Similar moment conditions can also be used to estimate the parameters of the multigroup. If time series data on $\{c_{\ell t}, i_{\ell t}\}$, for $\ell = 1, 2, \ldots, L$ (L is finite) are available, we can estimate the products, $\beta_{\ell\ell'}$, using the moment conditions (25), namely,

$$E\left(\frac{1 - c_{\ell,t+1}}{1 - c_{\ell t}} | \ \mathbf{i}_t\right) = \exp\left(-\sum_{\ell'=1}^{L} \beta_{\ell\ell'} i_{\ell' t}\right) + O\left(n^{-1}\right).$$

Then, as we have discussed in Section 5, $\beta_{\ell\ell'}$ is identifiable from (35) given γ and $\mathbf{w} = (w_1, w_2, \ldots, w_L)'$.

Under social interventions the recovery equation holds (since γ is unaffected), but the moment condition for c_{t+1} now depends on the time-varying transmission rate, β_t. For γ in the range of 1/14 to 1/21, it is reasonable to use 2 or 3 weeks rolling windows when estimating β_t. Consider

the case of a single group. For a window of size W, we have

$$\hat{\beta}_t(W) = \text{Argmin}_\beta \sum_{\tau=t-W+1}^{t} \left(\frac{1-c_\tau}{1-c_{\tau-1}} - e^{-\beta\, i_{\tau-1}} \right)^2. \tag{48}$$

To examine the finite sample properties of the rolling estimator, $\hat{\beta}_t(W)$, we conduct 2-weekly and 3-weekly rolling estimation using the simulated data with $n = 10,000$ under fixed, linearly declining and W-shaped transmission rates, respectively. We find that the 2-weekly and 3-weekly rolling estimates are very close to each other. The bias and RMSE are reasonably small in all scenarios. The results are provided in Tables S.1 and S.2, and Figure S.4 of the Online Supplement. We will hereafter focus on the 3-weekly rolling estimates.

7.2 Estimation allowing for measurement errors

It is widely recognized that in practice C_t and R_t (and $I_t = C_t - R_t$) are under-reported. The magnitude of under-reporting is measured by the multiplication factor (MF) in the literature (see, for example, Gibbons et al. (2014)). This multiple could change over time as the result of testing, but in any case it is certain that $\text{MF}_t > 1$. Denoting the observed values of c_t and i_t by $\tilde{c}_t$ and $\tilde{\imath}_t$, we have (we are assuming that $r_t = R_t/n = \text{MF}_t \tilde{r}_t$, where $\tilde{R}_t$ is the observed value of R_t)

$$c_t = \text{MF}_t \tilde{c}_t \quad \text{and} \quad i_t = c_t - r_t = \text{MF}_t \tilde{\imath}_t.$$

Then the moment condition in terms of observed values ($\tilde{c}_t$ and $\tilde{\imath}_t$) can be written as

$$E\left(1 - \text{MF}_{t+1}\tilde{c}_{t+1} | \, \tilde{\imath}_t, \tilde{c}_t\right) = \left(1 - \text{MF}_t \, \tilde{c}_t\right) e^{-\beta \text{MF}_t \, \tilde{\imath}_t}. \tag{49}$$

Suppose further that MF_{t+1} is a martingale process distributed independently of $\tilde{c}_{t+1}$, so that $E(\text{MF}_{t+1}) = \text{MF}_t$. In this case, it is easily seen that

$$\begin{aligned} E\left[\left(\text{MF}_{t+1} - \text{MF}_t\right)\tilde{c}_{t+1} | \, \tilde{\imath}_t, \tilde{c}_t\right] &= E\left\{E\left[\left(\text{MF}_{t+1} - \text{MF}_t\right)\tilde{c}_{t+1} | \tilde{c}_{t+1}, \tilde{\imath}_t, \tilde{c}_t\right] | \, \tilde{\imath}_t, \tilde{c}_t\right\} \\ &= E\left\{\tilde{c}_{t+1} E\left[\left(\text{MF}_{t+1} - \text{MF}_t\right) | \, \tilde{\imath}_t, \tilde{c}_t\right] | \, \tilde{\imath}_t, \tilde{c}_t\right\} \\ &= E\left(\tilde{c}_{t+1} | \, \tilde{\imath}_t, \tilde{c}_t\right) E\left[\left(\text{MF}_{t+1} - \text{MF}_t\right) | \, \tilde{\imath}_t, \tilde{c}_t\right] = 0, \end{aligned}$$

and then (49) becomes

$$E\left(1-\mathrm{MF}_t\ \tilde{c}_{t+1}|\ \tilde{\imath}_t,\tilde{c}_t\right)=\left(1-\mathrm{MF}_t\tilde{c}_t\right)e^{-\beta\mathrm{MF}_t\tilde{\imath}_t}.$$

Now noting that $\beta\tilde{\imath}_t\mathrm{MF}_t$ is likely to be quite small, we obtain

$$\begin{aligned}E\left(1-\mathrm{MF}_t\ \tilde{c}_{t+1}|\ \tilde{\imath}_t,\tilde{c}_t\right)&=\left(1-\mathrm{MF}_t\ \tilde{c}_t\right)e^{-\beta\mathrm{MF}_t\tilde{\imath}_t}\\&=\left(1-\mathrm{MF}_t\ \tilde{c}_t\right)\left(1-\beta\mathrm{MF}_t\tilde{\imath}_t+\frac{1}{2}\beta^2\mathrm{MF}_t^2\tilde{\imath}_t^2+....\right)\\&\approx 1-\mathrm{MF}_t\ \tilde{c}_t-\beta\mathrm{MF}_t\tilde{\imath}_t+\beta\mathrm{MF}_t^2\tilde{c}_t\tilde{\imath}_t+\ldots.\end{aligned}$$

Hence $E\left(\tilde{c}_{t+1}-\tilde{c}_t|\ \tilde{\imath}_t,\tilde{c}_t\right)\approx\beta\left(\tilde{\imath}_t-\mathrm{MF}_t\ \tilde{c}_t\tilde{\imath}_t\right)+\ldots$, and β and some average of MF_t can be estimated using rolling windows. However, in situations where $\tilde{c}_t$ and $\tilde{\imath}_t$ are very small (as is the case for the current pandemic), the second term in the above moment condition will be close to zero and it might not be possible to identify MF_t.

Remark 1 *Alternatively we could assume that MF_t itself is distributed independently of $\tilde{c}_t$, but allow MF_t to vary systematically with a measure of testing. It is expected that the data quality will improve as more testing is conducted. Given the current data availability, we leave the modelling of MF_t as a function of testing to future research.*

Figure 6 depicts the median of the 3-weekly estimates of β_t (scaled by $1/\gamma$) over $1,000$ replications with a MF of 1 (no under-reporting) and MF of 10, for the scenarios of linearly declining β_t and W-shaped β_t, respectively. It is notable that the estimates are reasonably close to the assumed value even if infected cases are under-reported 10 times. We have also considered MF $= 20$. The estimates are not displayed since they are so close to those under MF $= 10$ that the differences are hardly discernible. Also note that when β_t remains constant or rises, the estimates without measurement error (MF $= 1$) are closer to the assumed value than the estimates with measurement error; when β_t falls, however, the estimates under MF $= 10$ tend to be closer to the assumed value.

Let us close this section by addressing the concern about data smoothing. It is a common practice to take 1-week moving average (MA) of the recorded cases to mitigate daily fluctuation

Figure 6: Rolling estimates of β_t/γ under linearly declining and W-shaped transmission rates using different values of the multiplication factor (MF $= 1, 10$)

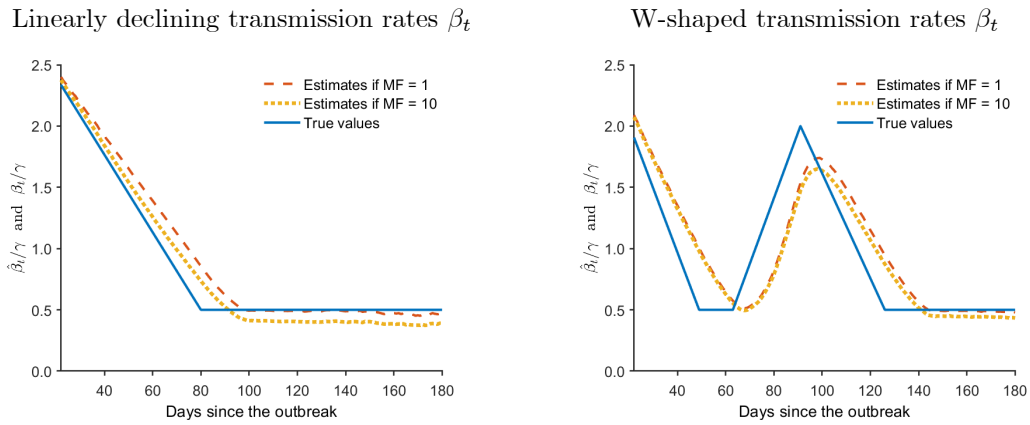

Notes: Estimates refer to the median of 3-weekly rolling estimates of β_t/γ computed using (48) over $1,000$ replications, where γ is set to $1/14$. The data were simulated using a single group model with the power law network. The mean number of contacts is $k = 10$. The exposure intensity parameter is $\tau_t = \beta_t/k$. Population size is $n = 10,000$.

due to reporting delays, weekend effects and other potential data anomalies. To investigate the effect of pre-filtering the data on the estimates of β_t, we apply a 1-week MA filter to the simulated data and compare the resulting estimates of β_t with the estimates obtained using unfiltered data. We find little difference in the estimates whether the data are filtered or not. (See Figure S.5 of the Online Supplement). But it is worth bearing in mind that filtering the data before estimation will introduce error serial correlation which could negatively affect the estimates. In practice it might be prudent to obtain estimates of β_t using filtered and unfiltered data. But since in our applications we obtain very similar results whether we use filtered or unfiltered data, we only report the estimates based on unfiltered observations.

8 Estimation of the recovery rate

As noted earlier, with reliable data on the number of removed (recovered or dead), the recovery rate, γ, can be estimated using the moment condition given by (22). In reality, however, it is hard to accurately measure R_t. In the calibration exercise to be presented in the next section, we do not estimate γ because the data on recovery are either unavailable or problematic in the countries we considered. In the current section we demonstrate that the recovery rate can be estimated very

precisely using simulated data. To simplify the exposition, we consider a single group ($L = 1$) and suppose that the time to recovery follows a geometric distribution as in the standard SIR model. The same aggregate outcome follows in the multigroup case when the probability of recovery is the same across all groups. Under these conditions the aggregate moment condition for recovery, (22), can be written as

$$\Delta R_{t+1} = \gamma I_t + u_{n,t+1}, \tag{50}$$

where $\Delta R_{t+1} = R_{t+1} - R_t$ and $u_{n,t+1}$ is a martingale difference process with respect to I_t and R_t. ($I_t = C_t - R_t$). Recall from (5) and (6) that $R_t = \sum_{i=1}^{n} y_{it}$ and $I_t = \sum_{i=1}^{n} z_{it}$, we note that $u_{n,t+1}$ is an aggregated error, namely, $u_{n,t+1} = \sum_{i=1}^{n} u_{i,t+1}$. Dividing both sides of (50) by n yields

$$\Delta r_{t+1} = \gamma i_t + \bar{u}_{n,t+1}, \tag{51}$$

where $\Delta r_{t+1} = r_{t+1} - r_t$, $r_t = R_t/n$, $i_t = I_t/n$ and $\bar{u}_{n,t+1} = n^{-1} \sum_{i=1}^{n} u_{i,t+1}$. For sufficiently large n and assuming that the individual differences in recovery are cross sectionally weakly correlated, we have $\bar{u}_{t+1} = O_p(n^{-1/2})$. It follows that γ can be consistently estimated from (51) by ordinary least squares (OLS) regression of Δr_{t+1} on i_t. Note that T is finite as $n \to \infty$. Due to the presence of $O_p\left(n^{-1/2}\right)$ in (51), it is expected that as n increases, the randomness will diminish and estimates of γ become increasingly precise. In the limit we would expect $\Delta r_{t+1} - \gamma i_t = O_p(n^{-1/2})$.

To examine the finite sample properties of the OLS estimator of γ, we simulate our model assuming a homogeneous recovery rate and compute the aggregate time series for $B = 1,000$ replications under a given population size, n. Denote the recovery and infection time series of the b^{th} replication by $r_{t+1}^{(b)}$ and $i_t^{(b)}$, respectively, for $b = 1, 2, \ldots, B$. For each replication, we obtain $\hat{\gamma}^{(b)}$ by regressing $\Delta r_{t+1}^{(b)}$ on $i_t^{(b)}$, without an intercept. As before, we run these regressions using the observations with $i_t^{(b)} \geq 0.01$, using the full sample as well as the three sub-samples (start, middle and end). The true value of γ in the experiment is set to $1/14$.

Table 2 reports the bias and RMSE of the OLS estimator of γ in (51). Note that even though the bias and RMSE in the table have been multiplied by 100, they are very small in magnitude. It is evident that we can estimate γ very precisely even with short time series samples. The RMSEs

Table 2: Finite sample properties of the moment estimator of γ

		Full	Sub-samples		
Population		Sample	Start	Middle	End
$n = 5,000$	Bias($\times$100)	0.0045	0.0097	0.0014	0.0049
	RMSE($\times$100)	0.1107	0.2019	0.1393	0.3496
$n = 10,000$	Bias($\times$100)	0.0034	0.0033	0.0023	0.0164
	RMSE($\times$100)	0.0765	0.1358	0.0968	0.2437
$n = 50,000$	Bias($\times$100)	0.0001	-0.0021	0.0011	0.0016
	RMSE($\times$100)	0.0347	0.0616	0.0436	0.1066
$n = 100,000$	Bias($\times$100)	0.0005	0.0022	-0.0002	-0.0022
	RMSE($\times$100)	0.0263	0.0435	0.0329	0.0780
T		110	37	36	38

Notes: The true value of γ is set to 1/14. The estimating equation is given by (51). Each sub-sample is about 1/3 of the full time series sample size. The time series sample sizes averaged across replications are reported in the last row. Number of replications is $B = 1,000$.

obtained by using the sub-samples are slightly larger than those obtained using the full sample; but they are still quite small given that the sub-samples are based on fewer than 40 observations. The RMSE declines as n increases – this confirms the theory that randomness will diminish with n at the rate of $n^{-1/2}$.

9 Calibrating the model to the Covid-19 evidence for selected European countries

We are now ready to calibrate our model to the realized Covid-19 data and perform counterfactual analyses. In view of the data quality and the current stage of the epidemic, we evaluate how our model matches with the recorded evidence in six European countries, namely, Austria, France, Germany, Italy, Spain and the United Kingdom. We first estimate the transmission rate, β_t, on data from these countries, which we then use to calibrate and evaluate our stochastic network model. The Covid-19 data are sourced from the repository of the Center for Systems Science and Engineering (CSSE) at Johns Hopkins University,[19] and the population data (for year 2019) are

[19] Available at `https://github.com/CSSEGISandData/COVID-19`.

obtained from the World Bank database.[20] To estimate β_t following (48), we need observations on per capita infected and active cases, c_t and i_t. Using the recorded number of infected cases, C_t, and population data, c_t is readily available. Since $I_t = C_t - R_t$, we can obtain i_t if the number of removed (recovered) cases, R_t, is available. Unfortunately, the recovery data is either not reported or subject to severe measurement error/reporting issues in many countries. For all six countries we therefore estimate the number of removed (including recoveries and deaths) by $R_t = (1-\gamma)\, R_{t-1} + \gamma C_{t-1}$, where the recovery rate γ is set to $1/14$, and the process starts from $R_1 = 0$. We then compute I_t by subtracting the estimated R_t from the recorded C_t.[21]

The Covid-19 outbreak in Europe began with Italy in early February 2020 with the recorded number of infections accelerating rapidly from February 21 onward. A rapid rise in infections took place about one week later in Spain, France and Germany, followed by UK and Austria at the end of February. Accordingly, we first compute 3-weekly rolling estimates of β_t using (48) over the period from mid-March onwards for Italy and about one week later for the other five countries, ending on October 15, 2020 (the last data point available used in this study). These estimates are then substituted in (44) to obtain estimates of the effective reproduction number given by $\hat{\mathcal{R}}_{et} = (1 - \text{MF} c_t)\, \hat{\beta}_t/\gamma$, where MF represents the extent of under-reporting of infected cases. As we shall see, MF differs across countries and is estimated to lie in the range of $3 - 9$. The evolution of the 3-weekly rolling estimates of $\hat{\mathcal{R}}_{et}$ over the period March–October for the six countries are displayed in Figure 7.[22] The epidemic tends to expand (contract) if $\hat{\mathcal{R}}_{et}$ is above (below) unity, and to highlight this property in Figure 7 we also show the dates for which $\hat{\mathcal{R}}_{et}$ falls below or rise above unity, as well as the start and end dates of the lockdowns.

Among the six countries, Italy started national lockdown on March 9, 2020, followed by Spain, Austria, and France about a week later, and Germany and UK two weeks later (on March 23,

[20] Available at `https://data.worldbank.org/indicator/SP.POP.TOTL`.

[21] Specifically, among the six countries, the recorded data on recovery are unavailable for Spain and UK; they are of poor quality for France and Italy; and they are relatively close to our estimated recovery for Austria and Germany. We have also calibrated our model using the recorded recovery data for Austria and Germany as a robustness check and obtained similar results.

[22] In early stages of the epidemic where c_t is small, estimates of $\hat{\mathcal{R}}_{et}$ and $\hat{\beta}_t/\gamma$ are very close, even if we set MF to 10. See Figure S.6 in the Online Supplement where estimates of $\hat{\mathcal{R}}_{et}$, are compared to $\hat{\beta}_t/\gamma$, for the six countries.

Figure 7: Rolling estimates of the effective reproduction numbers ($\mathcal{R}_{et}$) for selected European countries, with start and end dates of the respective lockdowns over the period March to October, 2020

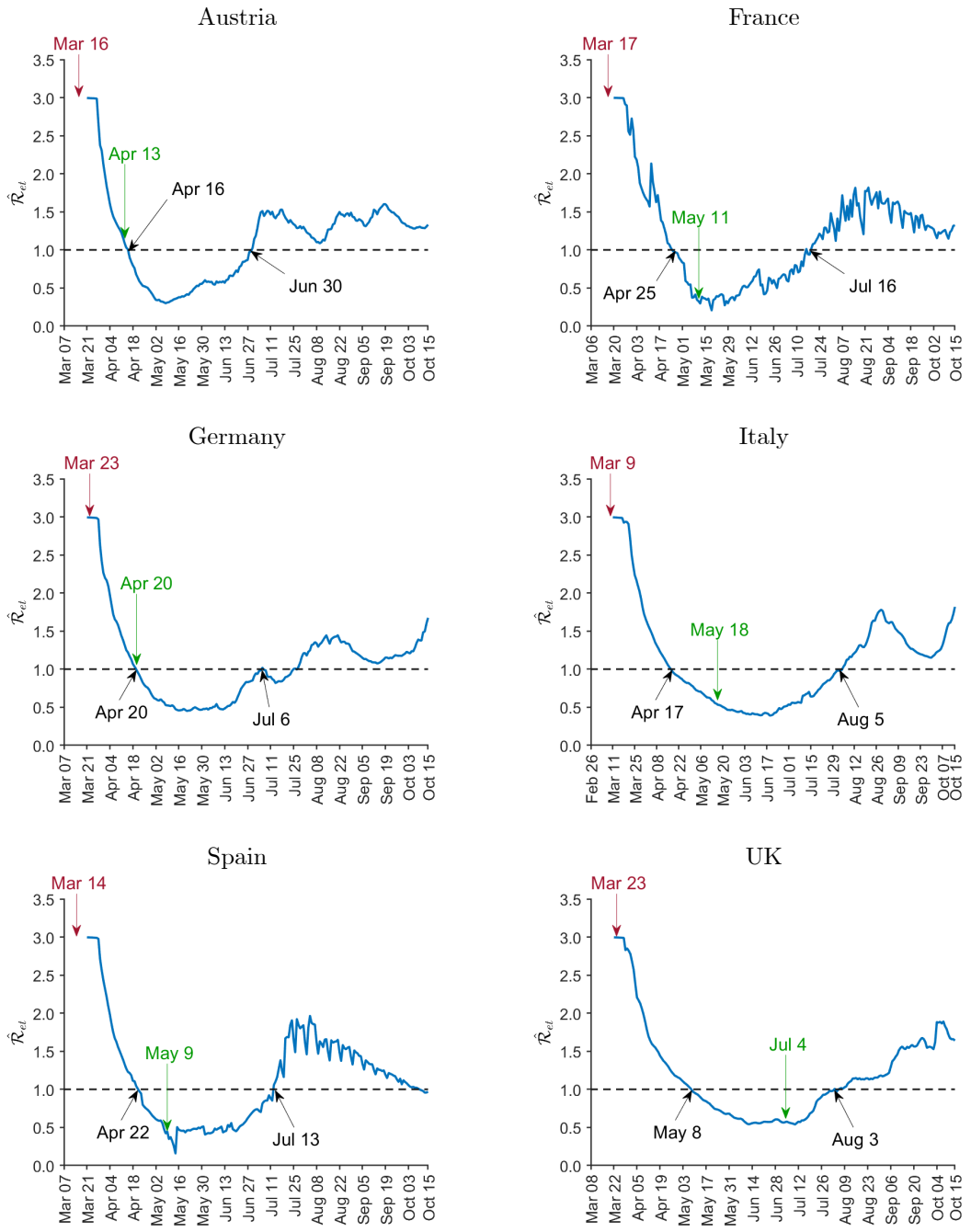

Notes: $\hat{\mathcal{R}}_{et} = (1 - \text{MF}c_t)\,\hat{\beta}_t/\gamma$, where $\gamma = 1/14$, $\hat{\beta}_t$ is the 3-weekly rolling estimate of β_t computed using (48), and the value of MF for each country is given in Figure 8. The number of removed (recoveries + deaths) is estimated recursively using $R_t = (1-\gamma)\,R_{t-1} + \gamma C_{t-1}$ for all countries, with $C_1 = R_1 = 0$. To render the calibrations comparable across the six countries, β is set to 3/14 (giving $\mathcal{R}_0 = 3$) during the first week of the epidemic. Red (green) arrows indicate the start (end) dates of the respective lockdowns. Black arrows indicate the dates when $\hat{\mathcal{R}}_{et}$ crosses one.

2020).[23] As can be seen from Figure 7, $\hat{\mathcal{R}}_{et}$ fell below one in mid to late April in all these countries except for the UK which took a bit longer before falling below unity in early May. On average it took 37 days to bring $\hat{\mathcal{R}}_{et}$ down below one from the start of lockdown, with Germany being the fastest (28 days) and UK being the slowest (46 days). By the end of May 2020, $\hat{\mathcal{R}}_{et}$ were brought down below 0.5 in all six countries except for the UK where the lowest value of $\hat{\mathcal{R}}_{et}$ (of about 0.54) occurred in early July. As lockdowns were eased, not surprisingly, the transmission rates started to rise, such that at the end of our sample (October 15, 2020) $\hat{\mathcal{R}}_{et}$ ended up at 1.3 or higher in all six countries with the exception of Spain.[24] This new surge in estimates of $\hat{\mathcal{R}}_{et}$ has led Austria, France, Germany and UK to announce second lockdowns, effective from late October or from early November.

Next we used the 3-weekly rolling estimates to calibrate the network SIR model to the Covid-19 evidence in these six countries. To render the calibrations comparable across these countries, we start the simulations with β set to 3/14 (giving $\mathcal{R}_0 = 3$) for the first week of the epidemic, and then set β_t to the rolling estimates computed from the realized data. As shown in Section 6, it makes little difference to the aggregate outcomes whether we carry out the simulations using single or multigroup models. Since we are interested in comparing the calibrated outcomes with realized cases, we conduct simulations using the single group model in this exercise. As before, we fix the average number of contacts to $k = 10$ and set the exposure intensity parameter to $\hat{\tau}_t = \hat{\beta}_t/k$; the population size in simulations is set to $n = 10,000$; the contact network is generated according to the power law specification with the number of contacts lying in the range of 5 to 50. All simulations start with 1/1000 of population randomly infected in day 1 and are replicated $B = 1,000$ times for each country.

Figure 8 presents the realized and calibrated cases. To match the realized proportion of infected cases with the calibrated ones, we compute the multiplication factor, MF, as the ratio of $c_{\max}$ between the calibrated and realized data for each country, and then plot the 7-day moving

[23] Lockdown dates across countries can be found in: `https://en.wikipedia.org/wiki/COVID-19_pandemic_lockdowns`.

[24] The estimates of $\hat{\mathcal{R}}_{et}$ seem to be reasonably robust to the choice of the estimation window. Similar estimates are obtained if a 2-weekly window is used. See Figure S.7 of the Online Supplement.

Figure 8: Realized and calibrated number of infected and active cases of Covid-19 for selected European countries

(a) Austria (MF = 4.82)

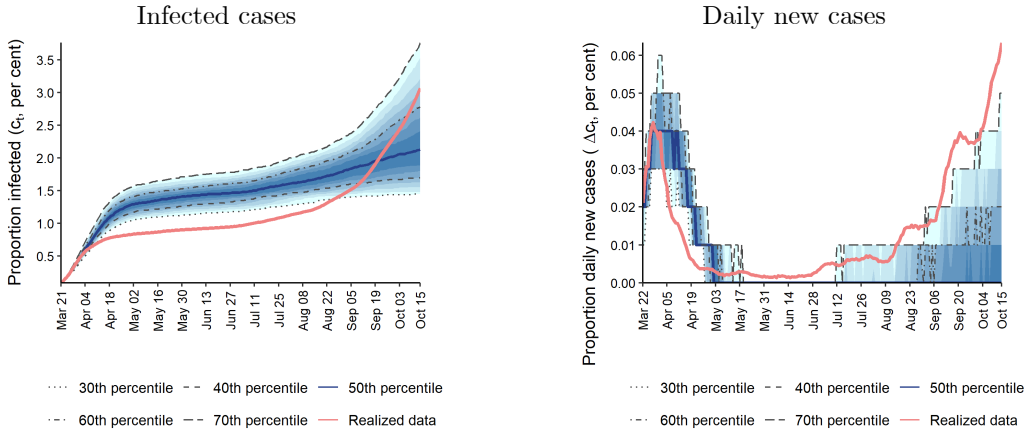

(b) France (MF = 5.16)

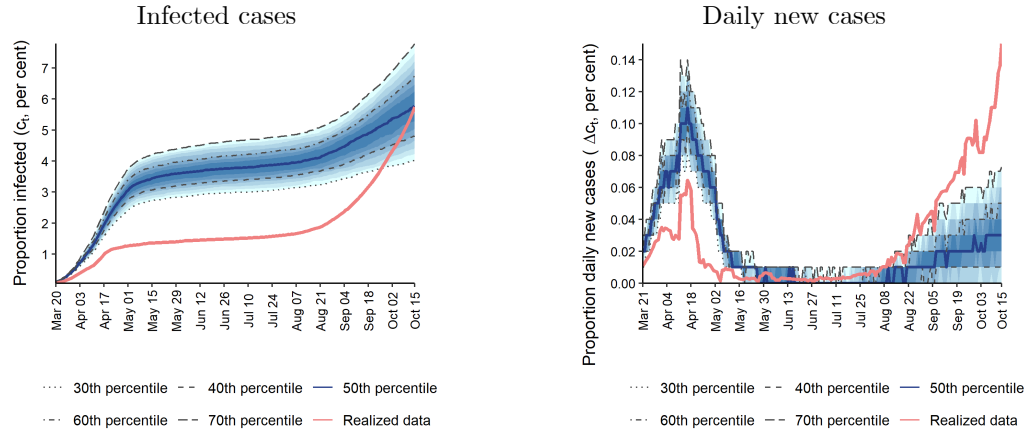

(c) Germany (MF = 8.26)

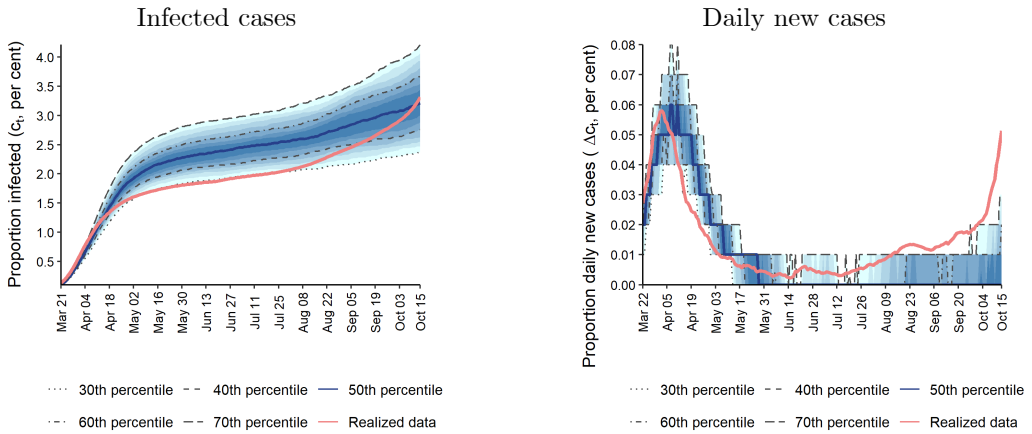

Figure 8: (Continued) Realized and calibrated number of infected and active cases of Covid-19 for selected European countries

(d) Italy (MF = 9.27)

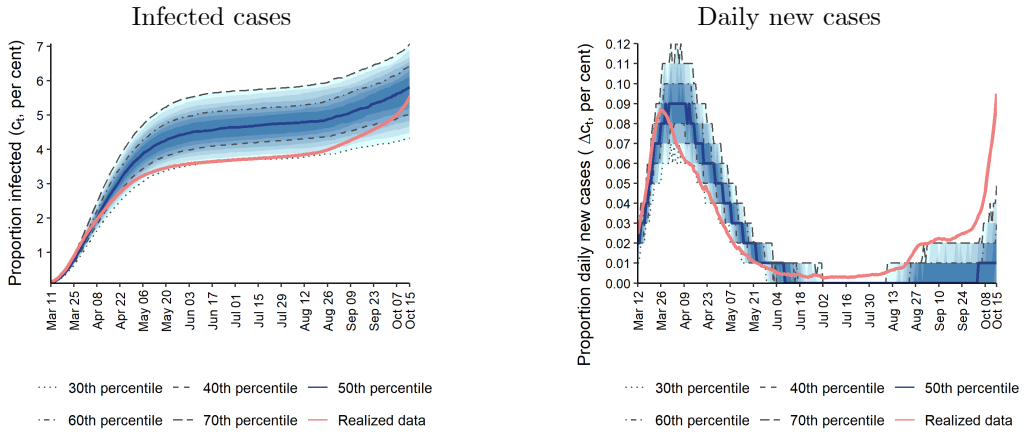

(e) Spain (MF = 2.60)

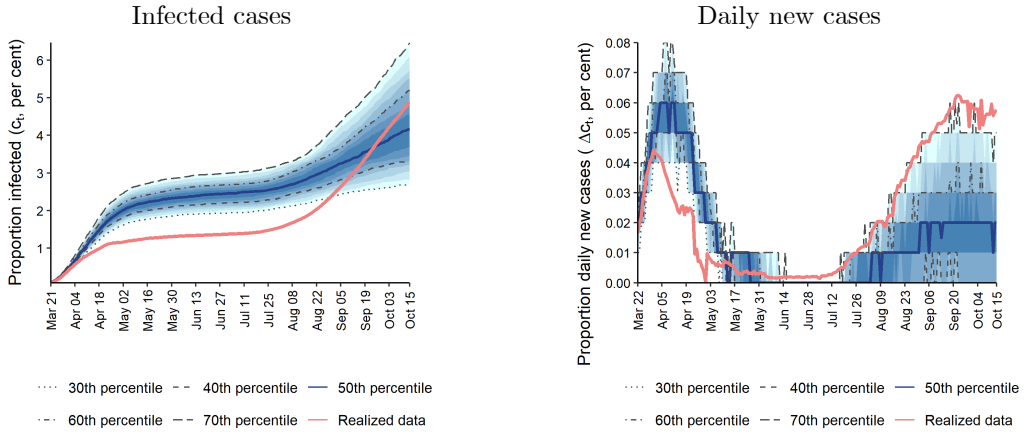

(f) UK (MF = 8.87)

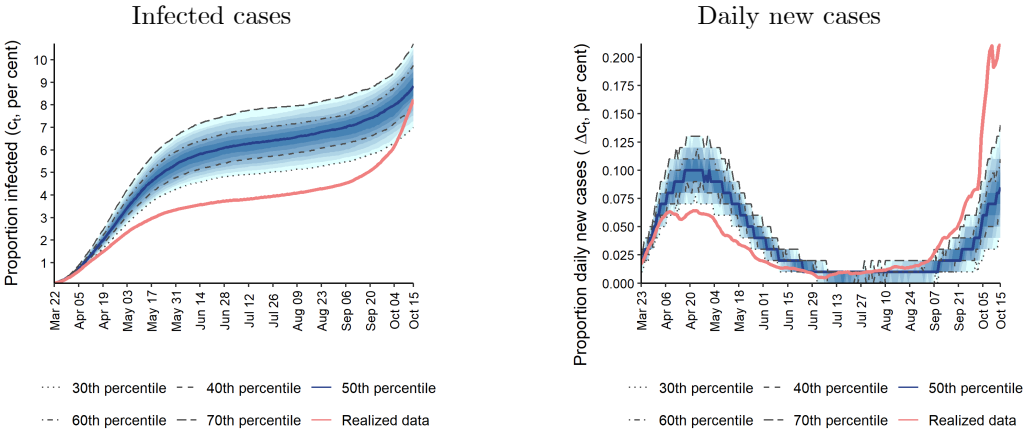

Notes: Realized series (7-day moving average) multiplied by the multiplication factor (MF) is displayed. MF is computed as the ratio of $c_{\max}$ between the calibrated and realized data. The number of removed (recoveries + deaths) is estimated recursively using $R_t = (1-\gamma)\,R_{t-1} + \gamma C_{t-1}$ for all countries, with $C_1 = R_1 = 0$. We set 1/1000 of the population randomly infected in day 1 and use a single group model with the power law network. The mean number of contacts is $k = 10$. The exposure intensity parameter is set to $\hat{\tau}_t = \hat{\beta}_t/k$, where $\hat{\beta}_t$ is the 3-weekly rolling estimate of β_t. $n = 10,000$. Number of replications is $1,000$.

average of realized data multiplied by the computed MF. Figure 8 also shows the proportion of daily new cases, which are the first differences of the proportion of infected cases after taking account of the under-reporting of infected cases. The calibrated data are displayed as fan charts with percentiles range from the 30^{th} to the 70^{th}. The estimates confirm significant evidence of under-reporting, with the estimated values of MF falling in the range of 3 to 9. These estimates are comparable to the degrees of under-reporting estimated by other approaches in recent studies, such as 7 times in China (Li et al., 2020); 3 to 16 times in five European countries, China and US (Jagodnik et al., 2020); 10 times in the US (Havers et al., 2020); and 10.5 times across 86 countries (Rahmandad, Lim, and Sterman, 2020), just to name a few. Once we have taken account of under-reporting, the calibrated cases match with the recorded cases fairly well. It is interesting that our model is able to catch the "second wave" of Covid-19 cases that start to show up in Europe from mid-August.

9.1 A Counterfactual Exercise

Having shown that the outcomes of the calibrated model closely match the evidence, we now show how the model can be used for specific counterfactual analysis of interest. Here we consider different outcomes that could have resulted from different timing of the lockdowns in Germany and the U.K.[25] In particular, we investigate the quantitative effect of bringing forward the lockdown in the UK on the infected cases, as compared to the effect of delaying the lockdown in Germany. To this end, we shift the estimated β_t values backward or forward for one or two weeks. We examine the counterfactual outcomes during the "first wave" of Covid-19 that levelled off in early July in both countries. As shown in Figure 9, if the German lockdown had been delayed by one week, the maximum proportion of infected cases would have increased from 2.5 to 5.8 percent, and the maximum proportion of active cases would have risen from 0.7 to 1.6 percent. In contrast, if the UK lockdown had been brought forward by one week, the model predicts that the maximum proportion of infected cases would have reduced from 6.2 to 2.6 percent, and the maximum number

[25] For example, Neil Ferguson, once an advisor to the UK government, stated on June 10 that "Had we introduced lockdown measures a week earlier, we would have reduced the final death toll by at least a half". See `https://www.politico.com/news/2020/06/10/boris-johnson-britain-coronavirus-response-312668`.

of active cases would have reduced from 1.3 to 0.5 percent. These results suggest that the UK could have achieved a similarly low level of infected cases per capita as Germany if it had implemented social distancing sooner. The maximum proportion of infected (active cases) is estimated to rise further to 12.8 (3.6) percent if the German lockdown was delayed by two weeks, and the maximum proportion of infected (active cases) is estimated to decrease further to 1.2 (0.3) percent if the UK lockdown was brought forward by two weeks.[26] In summary, this counterfactual exercise shows that it is critical to take measures to lower the effective reproduction number as early as possible, if a policy maker aims to control the accumulative and active number of infected cases.

10 Concluding Remarks

This paper has developed a stochastic network SIR model for empirical analyses of the Covid-19 pandemic across countries or regions. Moment conditions are derived for the number of infected and active cases for single as well as multigroup models. It is shown how these moment conditions can be used to identify the structural parameters and provide rolling estimates of the transmission rate at different stages of the epidemic. In empirical applications to six European countries, the estimates are shown to be robust to the well-known under-reporting of infected cases. The rolling estimates of the transmission rate are then used to calibrate the proposed epidemic model. It is shown that the simulated outcomes are reasonably close to the reported cases, once the under-reporting of infected is addressed. It is estimated that the number of reported cases could be between 3 to 9 times lower than the actual number of infected cases over the period from March to mid-October, 2020. The calibrated model is used for empirically-based counterfactual analyses. It is shown that the UK could have achieved an outcome similar to that experienced by Germany during the first wave if she had started the lockdown just one week earlier. Almost symmetrically, Germany would have experienced much higher infection rates (similar to the UK's experience) if she had started the lockdown one week later.

[26] See Figure S.8 of the Online Supplement.

Figure 9: Counterfactual number of infected and active cases for Germany and UK under different lockdown scenarios

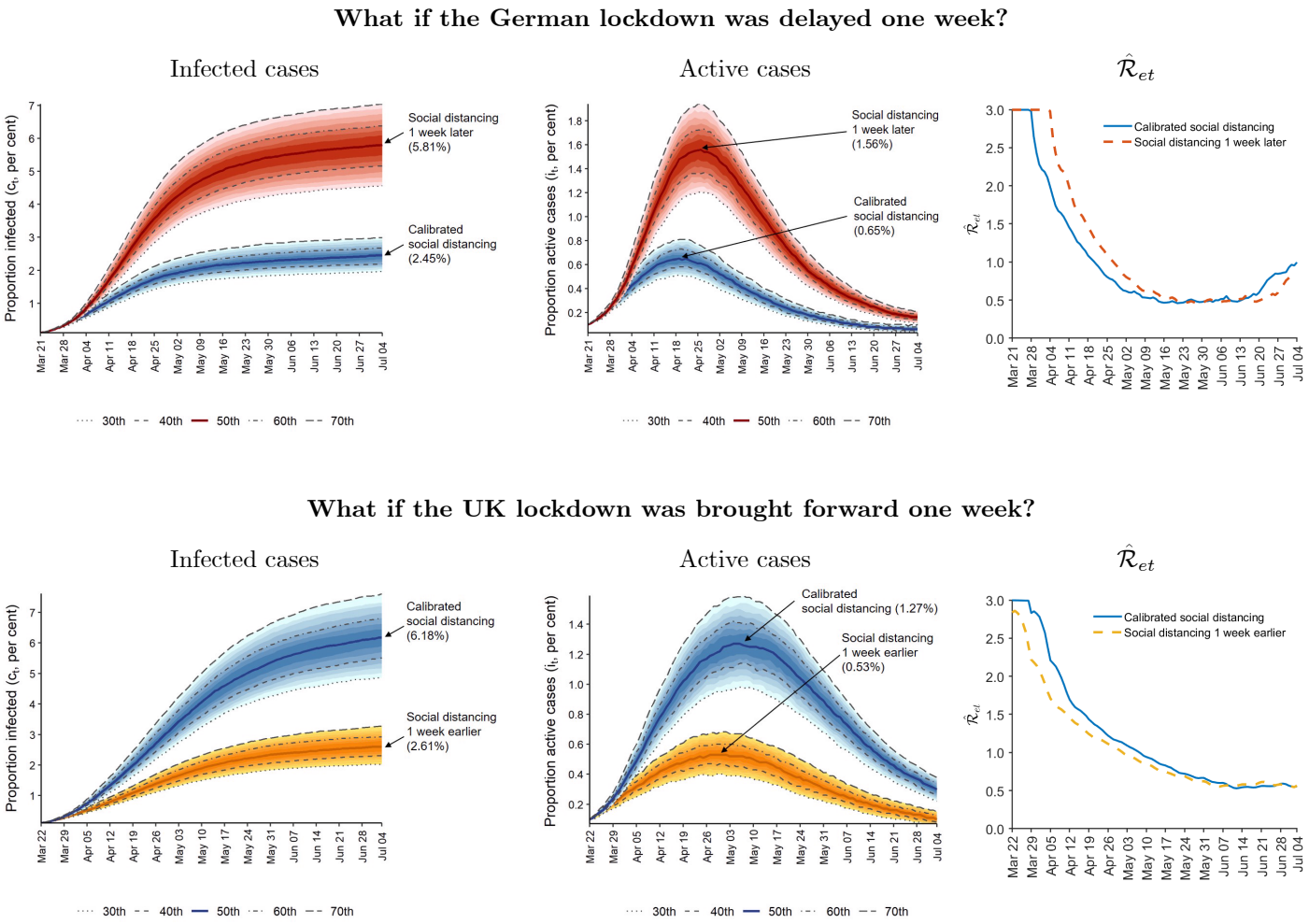

Notes: The simulation uses a single group model with power law network and begins with 1/1000 of the population randomly infected in day 1. $n = 10,000$. $k = 10$. $\gamma = 1/14$. $\hat{\tau}_t = \hat{\beta}_t/k$, where $\hat{\beta}_t$ is the 3-weekly rolling estimate computed using (48). The number of removed (recoveries + deaths) is estimated recursively using $R_t = (1-\gamma)\,R_{t-1} + \gamma C_{t-1}$ for both countries, with $C_1 = R_1 = 0$. The median of $\hat{\mathcal{R}}_{et}^{(b)} = \left(1 - c_t^{(b)}\right)\hat{\beta}_t/\gamma$ over 1,000 replications is displayed in the last column.

References

Acemoglu, D., V. Chernozhukov, I. Werning, and M. D. Whinston (2020). Optimal targeted lockdowns in a multi-group SIR model. NBER Working Paper No. 27102.

Akbarpour, M., C. Cook, A. Marzuoli, S. Mongey, A. Nagaraj, M. Saccarola, P. Tebaldi, S. Vasserman, and H. Yang (2020). Socioeconomic network heterogeneity and pandemic policy response. University of Chicago, Becker Friedman Institute for Economics Working Paper No. 2020-75.

Atkeson, A., K. A. Kopecky, and T. A. Zha (2020). Estimating and forecasting disease scenarios for COVID-19 with an SIR model. NBER Working Paper No. 27335.

Baqaee, D., E. Farhi, M. Mina, and J. H. Stock (2020). Policies for a second wave. *Brookings Papers on Economic Activity (forthcoming)*.

Beretta, E. and V. Capasso (1986). Global stability results for a multigroup SIR epidemic model. In T. G. Hallam, L. J. Gross, and A. Levin S (Eds.), *Mathematical Ecology*, pp. 317–340. World Scientific.

Bollobás, B. (1980). A probabilistic proof of an asymptotic formula for the number of labelled regular graphs. *European Journal of Combinatorics 1*(4), 311–316.

Chowell, G. and H. Nishiura (2008). Quantifying the transmission potential of pandemic influenza. *Physics of Life Reviews 5*(1), 50–77.

Chudik, A., M. H. Pesaran, and A. Rebucci (2020). Voluntary and mandatory social distancing: Evidence on COVID-19 exposure rates from Chinese provinces and selected countries. NBER working paper No. 27039.

D'Arienzo, M. and A. Coniglio (2020). Assessment of the SARS-CoV-2 basic reproduction number, R0, based on the early phase of COVID-19 outbreak in Italy. *Biosafety and Health*.

Del Valle, S. Y., J. M. Hyman, and N. Chitnis (2013). Mathematical models of contact patterns between age groups for predicting the spread of infectious diseases. *Mathematical Biosciences and Engineering 10*, 1475.

Ding, D., W. Qin, and X. Ding (2015). Lyapunov functions and global stability for a discretized multigroup SIR epidemic model. *Discrete & Continuous Dynamical Systems-B 20*(7), 1971.

Fernández-Villaverde, J. and C. I. Jones (2020). Estimating and simulating a SIRD model of COVID-19 for many countries, states, and cities. NBER working paper No. 27128.

Gibbons, C. L., M.-J. J. Mangen, D. Plass, A. H. Havelaar, R. J. Brooke, P. Kramarz, K. L. Peterson, A. L. Stuurman, A. Cassini, E. M. Fèvre, and M. E. Kretzschmar (2014). Measuring underreporting and under-ascertainment in infectious disease datasets: a comparison of methods. *BMC Public Health 14*(1), 147.

Guo, H., M. Y. Li, and Z. Shuai (2006). Global stability of the endemic equilibrium of multigroup SIR epidemic models. *Canadian Applied Mathematics Quarterly 14*(3), 259–284.

Harris, J. E. (2020). Overcoming reporting delays is critical to timely epidemic monitoring: The case of COVID-19 in New York City. *Preprint medRxiv*.

Havers, F. P., C. Reed, T. Lim, J. M. Montgomery, J. D. Klena, A. J. Hall, A. M. Fry, D. L. Cannon, C.-F. Chiang, A. Gibbons, et al. (2020). Seroprevalence of antibodies to SARS-CoV-2 in 10 sites in the United States, March 23-May 12, 2020. *JAMA Internal Medicine*.

Heffernan, J. M., R. J. Smith, and L. M. Wahl (2005). Perspectives on the basic reproductive ratio. *Journal of the Royal Society Interface 2*(4), 281–293.

Hethcote, H. W. (1978). An immunization model for a heterogeneous population. *Theoretical Population Biology 14*(3), 338–349.

Hethcote, H. W. (2000). The mathematics of infectious diseases. *SIAM Review 42*(4), 599–653.

Hoang, T., P. Coletti, A. Melegaro, J. Wallinga, C. G. Grijalva, J. W. Edmunds, P. Beutels, and N. Hens (2019). A systematic review of social contact surveys to inform transmission models of close-contact infections. *Epidemiology (Cambridge, Mass.) 30*(5), 723.

Hyman, J. M., J. Li, and E. A. Stanley (1999). The differential infectivity and staged progression models for the transmission of HIV. *Mathematical Biosciences 155*(2), 77–109.

Jagodnik, K., F. Ray, F. M. Giorgi, and A. Lachmann (2020). Correcting under-reported COVID-19 case numbers: estimating the true scale of the pandemic. *Preprint medRvix 14*.

Jarvis, C. I., K. Van Zandvoort, A. Gimma, K. Prem, P. Klepac, G. J. Rubin, and W. J. Edmunds (2020). Quantifying the impact of physical distance measures on the transmission of COVID-19 in the UK. *BMC Medicine 18*, 1–10.

Ji, C., D. Jiang, and N. Shi (2011). Multigroup SIR epidemic model with stochastic perturbation. *Physica A: Statistical Mechanics and its Applications 390*(10), 1747–1762.

Kermack, W. and A. McKendrick (1927). A contribution to the mathematical theory of epidemics. *Proceedings of the Royal Society of London. Series A. 115*(772), 700–721.

Kiss, I. Z., J. C. Miller, and P. L. Simon (2017). Mathematics of epidemics on networks. *Cham: Springer 598*.

Korolev, I. (2020). Identification and estimation of the SEIRD epidemic model for COVID-19. *Journal of Econometrics (forthcoming)*.

Lajmanovich, A. and J. A. Yorke (1976). A deterministic model for gonorrhea in a nonhomogeneous population. *Mathematical Biosciences 28*(3-4), 221–236.

Lee, C. and D. J. Wilkinson (2019). A review of stochastic block models and extensions for graph clustering. *Applied Network Science 4*(1), 122.

Leung, K., M. Jit, E. H. Lau, and J. T. Wu (2017). Social contact patterns relevant to the spread of respiratory infectious diseases in Hong Kong. *Scientific Reports 7*(1), 1–12.

Li, M. Y., Z. Shuai, and C. Wang (2010). Global stability of multi-group epidemic models with distributed delays. *Journal of Mathematical Analysis and Applications 361*(1), 38–47.

Li, R., S. Pei, B. Chen, Y. Song, T. Zhang, W. Yang, and J. Shaman (2020). Substantial undocumented infection facilitates the rapid dissemination of novel coronavirus (SARS-CoV-2). *Science 368*(6490), 489–493.

Matrajt, L. and T. Leung (2020). Evaluating the effectiveness of social distancing interventions to delay or flatten the epidemic curve of coronavirus disease. *Emerging Infectious Diseases 26*(8), 1740.

Miller, J. C. and I. Z. Kiss (2014). Epidemic spread in networks: Existing methods and current challenges. *Mathematical Modelling of Natural Phenomena 9*(2), 4–42.

Mossong, J., N. Hens, M. Jit, P. Beutels, K. Auranen, R. Mikolajczyk, M. Massari, S. Salmaso, G. S. Tomba, J. Wallinga, et al. (2008). Social contacts and mixing patterns relevant to the spread of infectious diseases. *PLoS Med 5*(3), e74.

Nepomuceno, E., D. F. Resende, and M. J. Lacerda (2018). A survey of the individual-based model applied in biomedical and epidemiology. *Journal of Biomedical Research and Reviews*.

Newman, M. (2018). *Networks*. Oxford University Press.

Nikbakht, R., M. R. Baneshi, A. Bahrampour, and A. Hosseinnataj (2019). Comparison of methods to estimate basic reproduction number (R0) of influenza, using Canada 2009 and 2017-18 A (H1N1) data. *Journal of Research in Medical Sciences 24*.

Obadia, T., R. Haneef, and P.-Y. Boëlle (2012). The R0 package: A toolbox to estimate reproduction numbers for epidemic outbreaks. *BMC Medical Informatics and Decision Making 12*(1), 1–9.

Pastor-Satorras, R., C. Castellano, P. Van Mieghem, and A. Vespignani (2015). Epidemic processes in complex networks. *Reviews of Modern Physics 87*(3), 925.

Rahmandad, H., T. Y. Lim, and J. Sterman (2020). Estimating COVID-19 under-reporting across 86 nations: implications for projections and control. Available at SSRN 3635047.

Rocha, L. E. and N. Masuda (2016). Individual-based approach to epidemic processes on arbitrary dynamic contact networks. *Scientific Reports 6*, 31456.

Thieme, H. R. (1983). Global asymptotic stability in epidemic models. In H. W. Knobloch and K. Schmitt (Eds.), *Equadiff 82 Proceedings*, pp. 608–615. Springer.

Thieme, H. R. (1985). Local stability in epidemic models for heterogeneous populations. In V. Capasso, E. Grosso, and S. L. Paveri-Fontana (Eds.), *Mathematics in Biology and Medicine*, pp. 185–189. Springer.

Thieme, H. R. (2013). *Mathematics in population biology*, Volume 12 of *Princeton Series in Theoretical and Computational Biology*. Princeton University Press.

Toda, A. A. (2020). Susceptible-infected-recovered (SIR) dynamics of COVID-19 and economic impact. Preprint arXiv: 2003.11221.

Willem, L., T. Van Hoang, S. Funk, P. Coletti, P. Beutels, and N. Hens (2020). SOCRATES: An online tool leveraging a social contact data sharing initiative to assess mitigation strategies for COVID-19. *Preprint medRxiv*.

Willem, L., F. Verelst, J. Bilcke, N. Hens, and P. Beutels (2017). Lessons from a decade of individual-based models for infectious disease transmission: a systematic review (2006-2015). *BMC infectious diseases 17*(1), 612.

Zhang, J., P. Klepac, J. M. Read, A. Rosello, X. Wang, S. Lai, M. Li, Y. Song, Q. Wei, H. Jiang, et al. (2019). Patterns of human social contact and contact with animals in Shanghai, China. *Scientific Reports 9*(1), 1–11.

Zhang, J., M. Litvinova, Y. Liang, Y. Wang, W. Wang, S. Zhao, Q. Wu, S. Merler, C. Viboud, A. Vespignani, et al. (2020a). Changes in contact patterns shape the dynamics of the COVID-19 outbreak in China. *Science*.

Zhang, J., M. Litvinova, Y. Liang, Y. Wang, W. Wang, S. Zhao, Q. Wu, S. Merler, C. Viboud, A. Vespignani, et al. (2020b). Supplementary materials for "Changes in contact patterns shape the dynamics of the COVID-19 outbreak in China". *Science*.

Zhou, J., Y. Yang, and T. Zhang (2017). Global stability of a discrete multigroup SIR model with nonlinear incidence rate. *Mathematical Methods in the Applied Sciences 40*(14), 5370–5379.

Online Supplement to "Matching Theory and Evidence on Covid-19 using a Stochastic Network SIR Model"

M. Hashem Pesaran
University of Southern California, USA, and Trinity College, Cambridge, UK

Cynthia Fan Yang
Florida State University

November 10, 2020

This Online Supplement provides technical derivations and presents additional simulation results. Section S1 generalizes the proposed stochastic network SIR model to allow for truncated geometric recovery. Section S2 discusses the edge probability and how the random networks were generated in our simulation exercises. Section S3 provides additional simulation results showing the robustness of the proposed model to the population size, n, and the network types. Section S4 reports additional Monte Carlo results of estimation of the transmission rate. Section S5 presents additional findings of the calibration and counterfactual analyses.

S1 Truncated Geometric Model of Recovery

Here we consider a generalization of the recovery model used in the main paper and suppose that for all individuals in group ℓ ($\ell = 1, 2, \ldots, L$) the time to recovery (or infection duration), denoted by $T^*_{i\ell,t} = t - t^*_{i\ell}$, follows a truncated geometric distribution with the probability mass distribution

$$\Pr\left(T^*_{i\ell,t} = t - t^*_{i\ell}\right) = A_\ell \left(1 - \gamma_\ell\right)^{t - t^*_{i\ell}}, \text{ for } t - t^*_{i\ell} = 1, 2, \ldots, \mathfrak{D}_\ell, \tag{S.1}$$

where $\mathfrak{D}_\ell$ is the maximum number of days for an individual to recover and is assumed to be the same for all individuals in group ℓ, γ_ℓ is the probability of recovery on each day if the geometric

distribution is non-truncated (i.e., $\mathfrak{D}_\ell \to \infty$). A_ℓ is a normalizing constant such that

$$A_\ell \sum_{\mathfrak{s}=1}^{\mathfrak{D}_\ell} (1-\gamma_\ell)^{\mathfrak{s}} = A_\ell \left[\frac{1-(1-\gamma_\ell)^{\mathfrak{D}_\ell}}{1-(1-\gamma_\ell)} \right] = 1,$$

which yields

$$A_\ell = \frac{\gamma_\ell}{1-(1-\gamma_\ell)^{\mathfrak{D}_\ell}}. \tag{S.2}$$

Then the "hazard function", denoted by $h_\ell(\mathfrak{s}, \mathfrak{D})$ ($\mathfrak{s} = 1, 2, \ldots, \mathfrak{D}$), defined as the probability of individuals in group ℓ recovering at time $\mathfrak{s}$ conditional on having remained infected for $\mathfrak{s}-1$ days is given by

$$\begin{aligned} h_\ell(\mathfrak{s}, \mathfrak{D}_\ell) &= \frac{\Pr(T^* = \mathfrak{s})}{\Pr(T^* > \mathfrak{s}-1)} = \frac{\Pr(T^* = \mathfrak{s})}{1-\Pr(T^* \leq \mathfrak{s}-1)} \\ &= \frac{A_\ell (1-\gamma_\ell)^{\mathfrak{s}-1}}{1-A_\ell \sum_{x=1}^{\mathfrak{s}-1} (1-\gamma_\ell)^x}. \end{aligned}$$

Now using (S.2) we have

$$h_\ell(\mathfrak{s}, \mathfrak{D}_\ell) = \frac{\gamma_\ell (1-\gamma_\ell)^{\mathfrak{s}-1}}{(1-\gamma_\ell)^{\mathfrak{s}-1} - (1-\gamma_\ell)^{\mathfrak{D}_\ell}}, \text{ for } \mathfrak{s} = 1, 2, \ldots, \mathfrak{D}_\ell.$$

Note that given a finite $\mathfrak{D}_\ell$ and $0 < \gamma_\ell < 1$, $h_\ell(\mathfrak{s}, \mathfrak{D}_\ell)$ monotonically increases with $\mathfrak{s}$. Hence, by assuming a truncated geometric distribution for recovery time, we are able to allow for the possibility that the longer an individual is infected the more likely s/he will recover. It is also clear that $h_\ell(\mathfrak{s}, \mathfrak{D}_\ell) \to \gamma_\ell$ as $D_\ell \to \infty$, which establishes the familiar result for a non-truncated geometric distribution used in the main paper. Under the truncated geometric distribution we have

$$\begin{aligned} &E\left[\zeta_{i\ell,t+1}(t^*_{i\ell}) \left| x_{i\ell,t}, y_{i\ell,t}, y_{i\ell,t-1}, \ldots, y_{i\ell,t^*_{i\ell}} \right.\right] \\ &= \Pr\left[\zeta_{i\ell,t+1}(t^*_{i\ell}) = 1 \left| x_{i\ell,t}, y_{i\ell,t} = 0, y_{i\ell,t-1} = 0, \ldots, y_{i\ell,t^*_{i\ell}} = 0 \right.\right] \\ &= h_\ell(t - t^*_{i\ell}, \mathfrak{D}_\ell), \end{aligned}$$

and the recovery process will be given by

$$E\left(R_{\ell,t+1}|R_{\ell t},C_{\ell t}\right)=R_{\ell,t}+\sum_{i=1}^{n_\ell}h_\ell\left(t-t_{i\ell}^*,\mathfrak{D}_\ell\right)\left(1-y_{i\ell,t}\right)x_{i\ell,t}$$
$$=R_{\ell,t}+\sum_{i=1}^{n_\ell}\frac{\gamma_\ell\left(1-\gamma_\ell\right)^{t-t_{i\ell}^*-1}}{\left(1-\gamma_\ell\right)^{t-t_{i\ell}^*-1}-\left(1-\gamma_\ell\right)^{\mathfrak{D}_\ell}}\left(1-y_{i\ell,t}\right)x_{i\ell,t}, \tag{S.3}$$

which does not simplify to the standard recovery process used in the SIR models, unless $\mathfrak{D}_\ell\to\infty$.

S2 Generating random networks

This section describes how we generated random draws from Erdős-Rényi and power law networks in the case of single and multigroup random networks used in our simulations.

First, in an Erdős-Rényi (ER) random graph each edge has a fixed probability of being present or not independently of all other edges. Specifically, we generate the ER random network with n nodes and a single group by considering all possible edges and including an edge between each distinct pair of nodes with probability $p=k/\left(n-1\right)$.

Second, we generate the power law random network in the case of a single group following the standard procedure in the literature:[S1] at each time t, we first draw a degree sequence from the (truncated) power law distribution given by (45), and then generate a network with that degree sequence based on a configuration model.[S2] Specifically, we draw a degree sequence $k_i\left(t\right)$ randomly and independently over i for $i=1,2,\cdots,n$, (with replacement), such that $k_i\left(t\right)$ realizes with probability p_{k_i}. Then we generate a configuration model with the degree sequence $\{k_i\left(t\right)\}$ by the standard algorithm – first assign each node with a number of stubs (half edges) that is equal to its degree, then match two stubs uniformly at random to form an edge and continue until all stubs are matched. Since the number of edges, denoted by $m\left(t\right)$, in a graph satisfies $2m\left(t\right)=\sum_i k_i\left(t\right)$, the generated degrees must add to an even number to be able to construct a graph. If the generated degrees add to an even number, we simply throw them away and generate another sequence. Also notice that this algorithm may produce self-loops and multi-edges. This

[S1] See, for example, Kiss et al. (2017), p. 20.

[S2] A configuration model is a model of a random graph with a given degree sequence. The name "configuration" originates from Bollobás (1980) meaning arrangements of edges in the model.

is not a concern if n is sufficiently large, since the density of such problematic links is of order $O(n^{-1})$.[S3] In simulations, we discard self-loops and collapse multi-edges. The resulting graph is used as the power law contact network for time t and the same procedure is repeated in each t and over replications.

It follows from the degree distribution given by (45) that the normalizing constant has the expression $C = \left(\sum_{k_{\min}}^{k_{\max}} x^{-\alpha}\right)^{-1}$, and then the average degree of the power law graph is

$$k = E(x) = \sum_{k_{\min}}^{k_{\max}} xp(x) = C \sum_{k_{\min}}^{k_{\max}} x^{1-\alpha} = \left(\sum_{k_{\min}}^{k_{\max}} x^{-\alpha}\right)^{-1} \left(\sum_{k_{\min}}^{k_{\max}} x^{1-\alpha}\right). \tag{S.4}$$

In simulations the value of the exponent, α, is solved from (S.4) such that $k = 10$.

Given the degree sequence $\boldsymbol{k}(t) = [k_1(t), k_2(t), \ldots, k_n(t)]'$, the (conditional) edge probability between node i and node j in the configuration model is[S4]

$$E[d_{ij}(t) \mid \boldsymbol{k}(t)] = \frac{k_i(t) k_j(t)}{2m(t) - 1},$$

which in the limit of large $m(t)$ can be rewritten as

$$E[d_{ij}(t) \mid \boldsymbol{k}(t)] = \frac{k_i(t) k_j(t)}{2m(t)} = \frac{k_i(t) k_j(t)}{\sum_{r=1}^{n} k_r(t)} = \frac{k_i(t) k_j(t)}{nk}.$$

Since $k_i(t)$ and $k_j(t)$ are independent draws from the power law distribution with mean k, the (unconditional) edge probability is

$$p_{ij} = E[d_{ij}(t)] = E\{E[d_{ij}(t) \mid \boldsymbol{k}(t)]\} = \frac{k^2}{nk} = \frac{k}{n},$$

which is the same as the edge probability in the ER random network.

Finally, the network with multigroup can be generated following the stochastic block model (SBM), which is a popular random graph model for blocks (groups, or communities) in networks.[S5] Recall our assumption that the probability of contacts is homogeneous within groups but different across groups. Node (or individual) i in group ℓ is denoted by (i, ℓ). At each time t, we draw a network in which the edge between each distinct pair of nodes, (i, ℓ) and $\left(j, \ell'\right)$, exists with

[S3] A proof can be found in Newman (2018), pp. 373–375.

[S4] See, e.g., Newman (2018), p. 373.

[S5] A recent review of stochastic block models is provided by Lee and Wilkinson (2019).

probability $p_{\ell\ell'}$. That is, the edge probabilities depend on the groups which nodes belong to. We set the within group probability $p_{\ell\ell} = k_{\ell\ell}/(n_\ell - 1) \approx k_{\ell\ell}/n_\ell$, and the between group probability $p_{\ell\ell'} = k_{\ell\ell'}/n_{\ell'}$. By construction we have $p_{\ell\ell'} = p_{\ell'\ell}$ under the reciprocity condition, $n_\ell k_{\ell\ell'} = n_{\ell'} k_{\ell'\ell}$. Note that if $p_{\ell\ell'} = p$ for all groups ℓ and ℓ', the SBM reduces to the ER random graph. If $p_{\ell\ell'}$ are not all identical, the SBM generates ER random graphs within each group and random bipartite graphs between groups. Accordingly, the degree distribution of the generated network is a mixture of Poisson degree distributions. To create heavy-tailed degree distributions or other types of degree heterogeneity, one can generalize the SBM analogous to the configuration model or consider the degree-corrected SBM, but these generalizations are beyond the scope of the current paper.[S6]

S3 Simulated properties of the stochastic network SIR model

First we consider how the simulated properties of the proposed model vary as we increase the population size, n. Specifically, we carry out simulations with $n = 10,000$, $50,000$, and $100,000$ assuming a fixed transmission rate, where the parameters take the same values as set out in Section 6.1 of the paper, namely $k = 10$, $\gamma = 1/14$, $\mathcal{R}_0 = 3$, $\beta = \gamma\mathcal{R}_0 = 3/14$, and $\tau = \beta/k$. For each replication the simulation is initialized with 1/1000 of the population randomly infected in day 1. The number of replications is set to $B = 1,000$, for all experiments. Figure S.1 displays the proportions of infected and active cases, as well as $c_{\max} = B^{-1}\sum_{b=1}^{B} \max_t \left(c_t^{(b)}\right)$ and $i_{\max} = B^{-1}\sum_{b=1}^{B} \max_t \left(i_t^{(b)}\right)$, below the respective epidemic curves. As can be seen, the simulated values of $c_{\max}$ and $i_{\max}$ are hardly affected by the choice of n in the range of $(10,000,\ 100,1000)$. The time at which active cases peak is also almost the same across n. Although uncertainty in the simulation results decreases with larger n, the interquartile range with $n = 10,000$ is quite tight. Therefore, without loss of generality and to save computational time we set $n = 10,000$ in all experiments below and those reported in the main paper.

[S6] See, for example, Newman (2018), Section 12.11.16, for a discussion.

Figure S.1: Simulated number of infected and active cases using a single group model with $\mathcal{R}_0 = 3$ under different population sizes

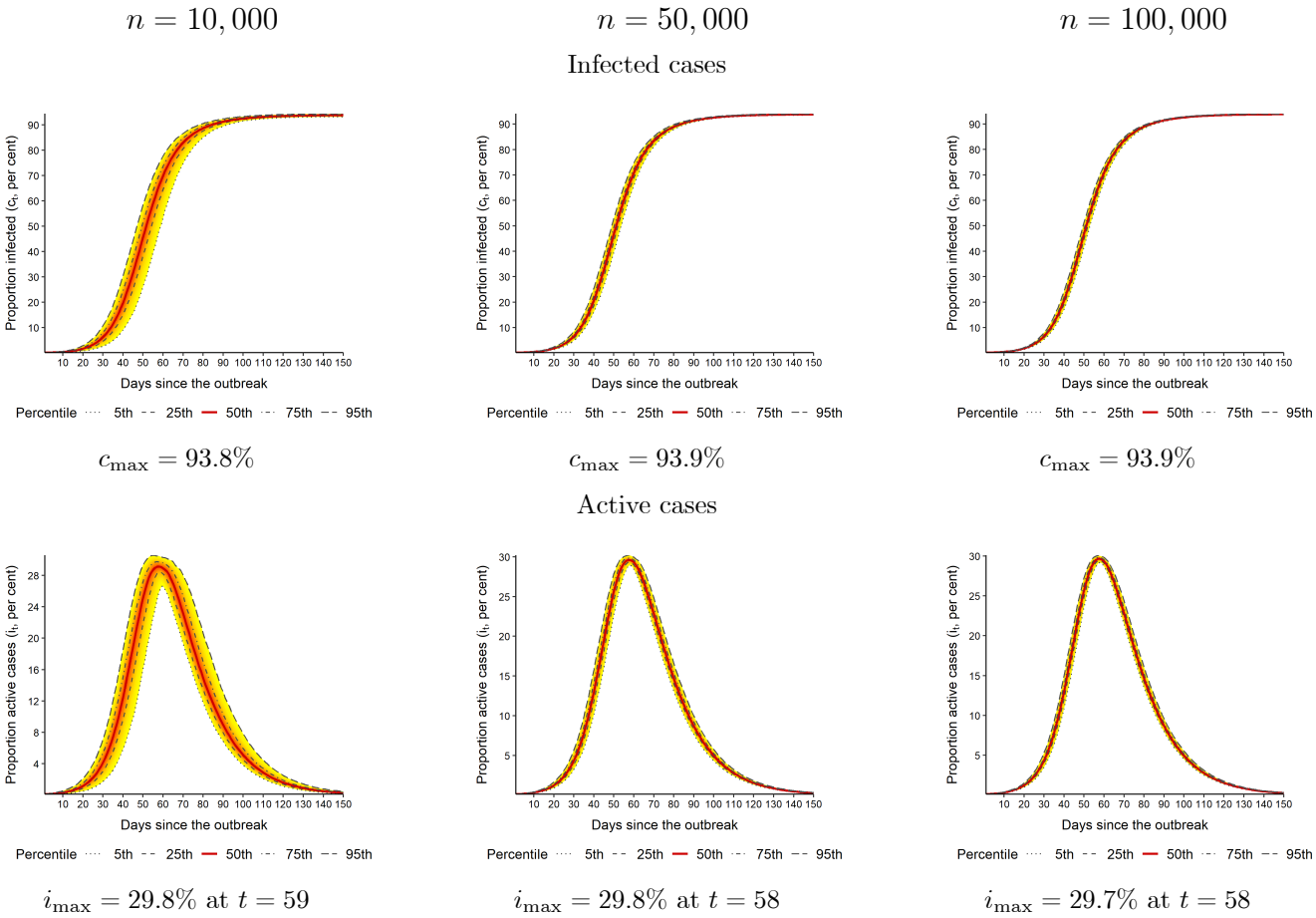

Notes: We set 1/1000 of the population randomly infected in day 1 and use the power law network with mean contact number $k = 10$. The recovery rate is $\gamma = 1/14$. The exposure intensity parameter is $\tau = \gamma\mathcal{R}_0/k$. Number of replications is $1,000$.

We next examine the effect of network topology on the simulation results. In particular, we consider two widely used random networks – the Erdős-Rényi (ER) and the power law random networks. Figure S.2 illustrates the two networks with $n = 50$ nodes and the same average degree, $k = 10$. It is assumed that the minimum and maximum degrees of the power law network is $k_{\min} = 5$ and $k_{\max} = 49$, respectively. The networks were generated following the algorithms described in Section S2 of this Online Supplement. Note that the ER random network has a binomial degree distribution, and it can be seen from the figure that most nodes have comparable degrees with the mean degree of 10, approximately. In contrast, the power law network has a heavy-tailed degree distribution, and there are many small-degree nodes as well as a few highly

Figure S.2: Examples of power law and Erdos-Renyi random networks

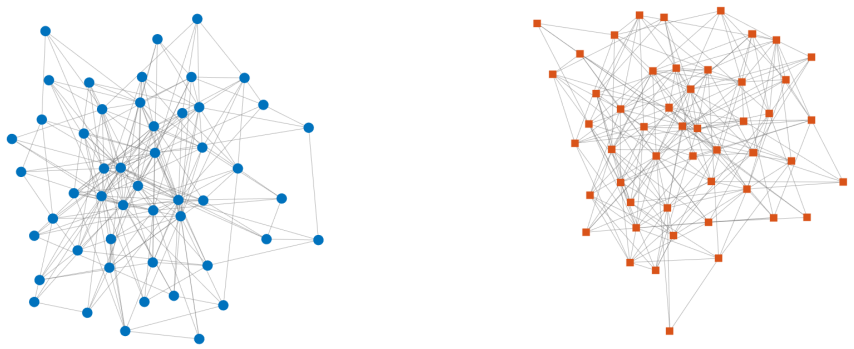

Notes: $n = 50$. Mean degree is $k = 10$ in both networks. The degree distribution in the power law network follows $p_x = Cx^{-2.43}$, for $x = 5, 6, \ldots, 49$.

connected nodes in the graph. Figure S.3 compares the simulation results obtained using the two random networks with the same average degree of 10. We set $k_{\min} = 5$ and $k_{\max} = 50$ for the power law networks. The values of γ, $\mathcal{R}_0$, and τ, and initialization of the simulation process are as given above. We plot the proportion of infected and active cases with uncertainty bands, and also the median values across replications for easy comparison. It is clear from Figure S.3 that the median epidemic curves obtained by the two different random networks overlap. Although not shown, the mean simulation results are very close to the median values for both types of networks. We therefore focus on the power law network (viewed as more realistic) in our simulation and calibration exercises.

S4 Estimation of the transmission rate

Here we provide further evidence on the performance of the rolling estimators of the transmission rates. Table S.1 below reports the finite sample properties of the rolling estimates of $\mathcal{R}_0$ in the case where it is fixed at $\mathcal{R}_0 = 3$ and the population size is $n = 10,000$, which complements Table 1 of the paper. The simulated data were obtained under the same set-up as that for Table 1, and are based on a single group model with the power law network, and the parameter values

Figure S.3: Simulated number of infected and active cases using a single group model with $\mathcal{R}_0 = 3$ under different network topologies

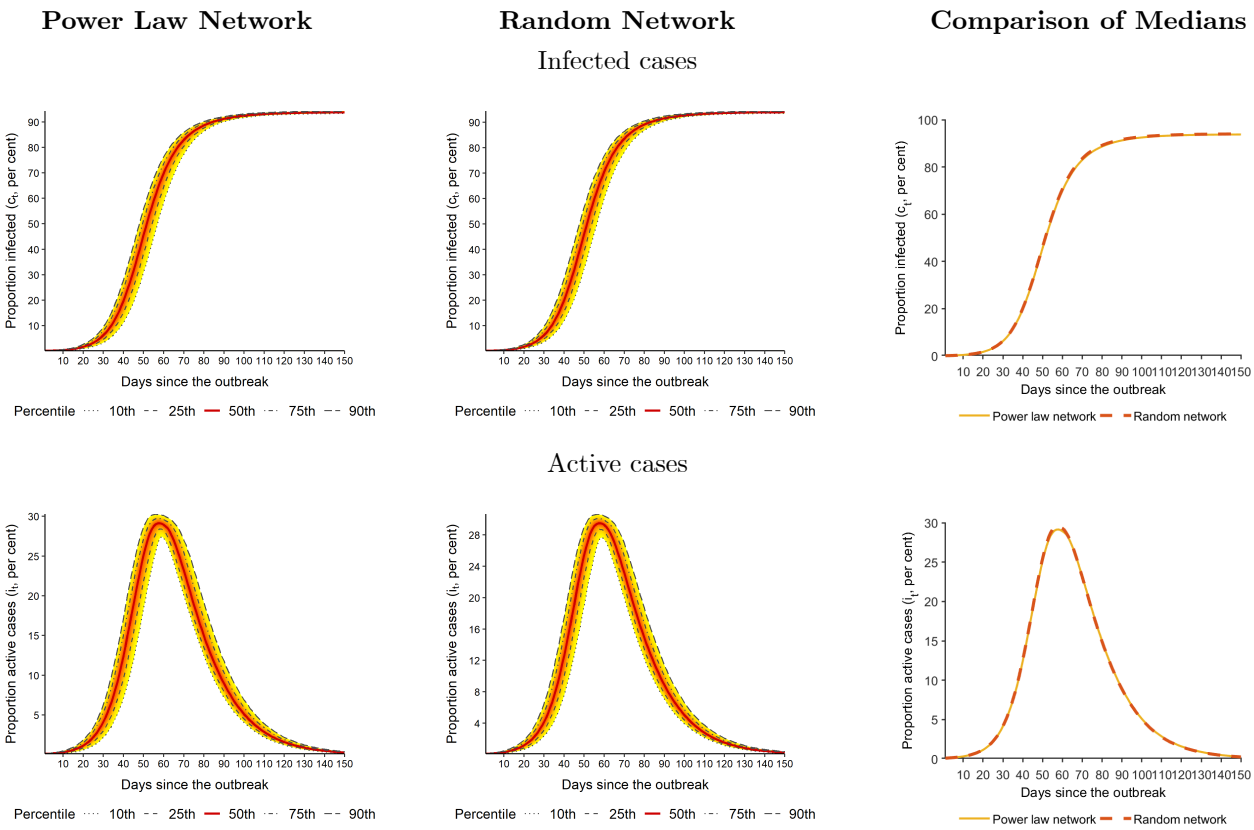

Notes: We set 1/1000 of the population randomly infected in day 1. Both networks have mean degrees $k = 10$. The recovery rate is $\gamma = 1/14$. The exposure intensity parameter is $\tau = \gamma \mathcal{R}_0 / k$. Population size is $n = 10,000$. Number of replications is $1,000$.

$k = 10$, $\gamma = 1/14$, and $\beta = 3/14$. Table S.1 presents the bias and root mean square error (RMSE) of the rolling estimates, $\hat{\mathcal{R}}_0(W) = \hat{\beta}_t(W)/\gamma$, where the window size, W, is set to 2 and 3 weeks, respectively, and $\hat{\beta}_t(W)$ is computed based on (48) of the main paper. The results refer to averages computed over the full sample ($4^{th} - 15^{th}$ weeks after the outbreak), as well as over the four non-overlapping 3-weekly sub-samples.

As to be expected, the bias remains small and similar over different sub-samples. The RMSE is smaller in the middle of the epidemic than at the beginning and end stages where i_t is very close to zero. Note that unlike Table 1 of the main paper, we do not discard observations with $i_t < 0.01$ in order to show that the transmission rate cannot be estimated very precisely at the early and late stages of the epidemic. Therefore the RMSEs in early and end sub-samples are

Table S.1: Finite sample properties of the rolling estimates of $\mathcal{R}_0$, in the case where it is fixed at $\mathcal{R}_0 = 3$

		Full sample	3-weekly sub-samples			
Weeks since the outbreak		$4^{th} - 15^{th}$	$4^{th} - 6^{th}$	$7^{th} - 9^{th}$	$10^{th} - 12^{th}$	$13^{th} - 15^{th}$
2-weekly rolling estimates	Bias	-0.031	-0.028	-0.034	-0.040	-0.024
	RMSE	0.124	0.157	0.068	0.089	0.184
3-weekly rolling estimates	Bias	-0.033	-0.031	-0.033	-0.042	-0.027
	RMSE	0.105	0.155	0.063	0.072	0.129

Notes: The rolling estimates are computed using (48) of the main paper. The true value of $\mathcal{R}_0$ is set to β/γ, where $\beta = 3/14$ and $\gamma = 1/14$ so that $\mathcal{R}_0 = 3$. Population size is $n = 10,000$. Number of replications is $1,000$.

larger than those in Table 1 of the main paper. Nonetheless, the average RMSE of $\hat{\mathcal{R}}_0$ over the full period lies in the range $0.11 - 0.12$, which is reasonably small compared to the true value of 3. In addition, the properties of the 2-weekly and 3-weekly rolling estimates are very close, with the 3-weekly rolling estimates having slightly smaller RMSE as compared to the 2-weekly estimates.

We now turn to the performance of the rolling estimates under linearly declining β_t and W-shaped β_t scenarios. The simulations are described in Section 6.2 of the paper. Figure S.4 compares the 2-weekly and 3-weekly rolling estimates of β_t/γ using the simulated data. The figure displays the median estimates based on $1,000$ replications, as well as the assumed value of β_t. It is readily seen that the 2-weekly and 3-weekly rolling estimates are very close. As β_t changes over time, the rolling estimates catch up with the true values of β_t with a time lag, and as to be expected 2-weekly rolling estimates tend to catch up more quickly. When the assumed value falls (rises), $\hat{\beta}_t$ slightly overestimates (underestimates) β_t, with negligible sampling errors when β_t is fixed.

The magnitude of the bias and RMSE in estimating β_t/γ are summarized in Table S.2, which complements the pictorial representation of the results in Figure S.4. Full sample comprises observations over 180 days since the outbreak. We also divide the full sample into sub-samples in which β_t declines, stays constant, or rises, which only applies to the case of W-shaped β_t. We report the average bias and RMSE of $\hat{\beta}_t/\gamma$ for the full sample and each sub-sample. Since there are two declining periods (weeks $1 - 7$ and $13 - 18$) in the case of W-shaped β_t, the bias and RMSE for the declining sub-sample refer to the values averaged over the two periods over which

Figure S.4: Rolling estimates of β_t/γ under 2- and 3-weekly rolling windows

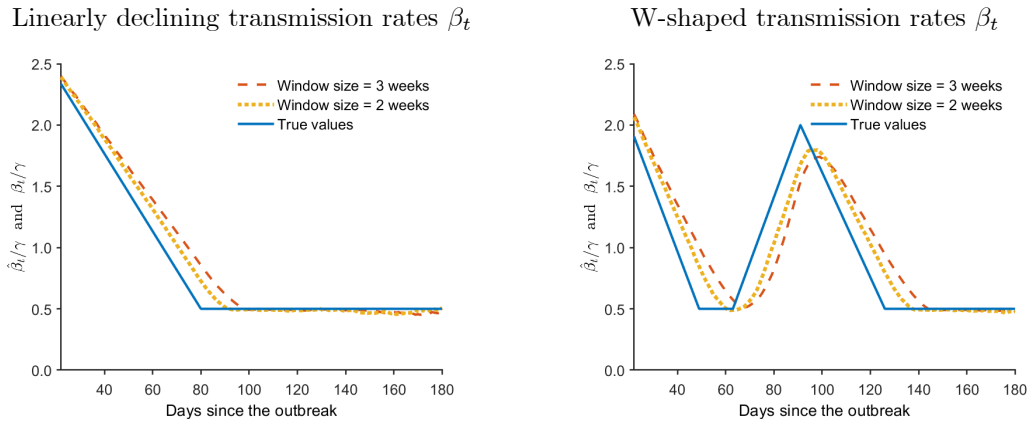

Notes: Median estimates over $1,000$ replications are shown in the figure. The rolling estimates are computed using (48) of the main paper. The data were simulated using a single group model with the power law network. The mean number of contacts is $k = 10$. The exposure intensity parameter is $\tau_t = \beta_t/k$. Population size is $n = 10,000$.

β_t is falling. Similarly, results for the fixed β_t sub-sample in the case of W-shaped β_t refer to the estimates averaged over the weeks $8-9$ and $19-26$.

The average bias and RMSE over the full sample are found to be reasonably small, with the rolling estimates having positive (negative) bias when the true transmission rate is decreasing (increasing), which are in line with the estimates depicted in Figure S.4. The bias and RMSE are much smaller when the transmission rate is steady, compared to when the transmission rate is changing. The 2-weekly rolling estimates have smaller bias and RMSE as compared to the 3-weekly rolling estimates when β_t is declining. Over the full sample, the 2-weekly rolling estimates slightly outperform the 3-weekly estimates in both scenarios of varying transmission rates. Overall, both 2-weekly and 3-weekly rolling estimates are quite close and perform well.

Finally, we show that the rolling estimates of β_t are robust to whether a moving average (MA) filter is applied to the data before estimation. In practice, a 1-week MA filter is often applied when displaying infected cases in order to smooth out data irregularities and to alleviate the influence of delayed reporting. It is therefore of interest to see whether the estimated β_t are robust to the application of an MA filter to the data. Figure S.5 presents the results. It can be seen that whether the data is filtered or not leads to very similar estimates of β_t, and the estimates are also reasonably close to the assumed value in both scenarios of linearly declining β_t and W-shaped β_t.

Table S.2: Finite sample properties of the rolling estimates of β_t/γ, in the case of linearly declining and W-shaped transmission rates

		Full Sample	Sub-samples		
			Declining β_t	Fixed β_t	Rising β_t
Linearly declining transmission rates β_t					
2-weekly rolling estimates	Bias	0.055	0.130	0.005	-
	RMSE	0.174	0.208	0.151	-
3-weekly rolling estimates	Bias	0.085	0.206	0.014	-
	RMSE	0.175	0.243	0.135	-
W-shaped transmission rates β_t					
2-weekly rolling estimates	Bias	0.041	0.194	0.033	-0.322
	RMSE	0.241	0.282	0.146	0.368
3-weekly rolling estimates	Bias	0.067	0.264	0.095	-0.443
	RMSE	0.291	0.340	0.171	0.470

Notes: Reported are the average bias and RMSE over the full sample (180 days) and sub-samples in which the transmission rate declines, remains fixed, or rises. The declining (fixed) sub-samples in the case of W-shaped transmission rates give averages over declining (fixed) periods. The rolling estimates are computed using (48) in the main paper. The data were simulated using a single group model with the power law network. The mean number of contacts is $k = 10$. The exposure intensity parameter is $\tau_t = \beta_t/k$. Population size is $n = 10,000$. Number of replications is $1,000$.

Figure S.5: Comparison of rolling estimates of β_t/γ using unfiltered and one-week moving average filtered data

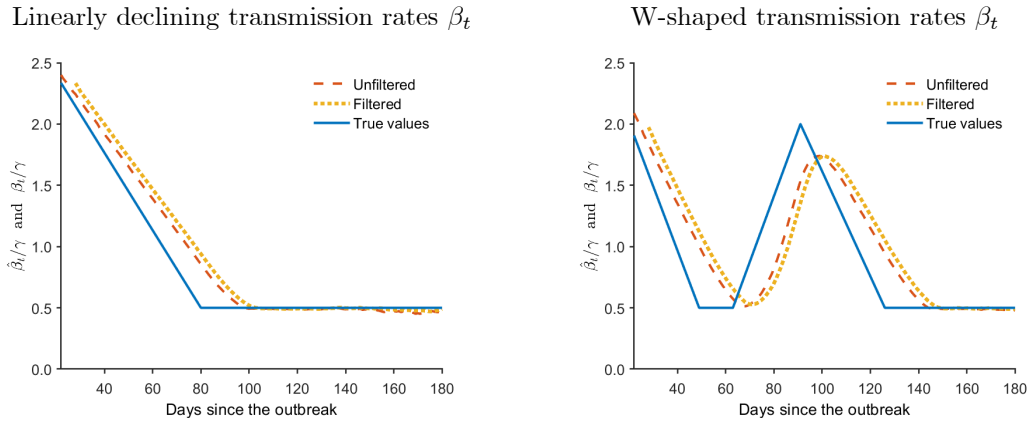

Notes: The median of 3-weekly rolling estimates over $1,000$ replications are shown in the figure. The estimates using filtered data are based on 1-week moving average filtered observations. The rolling estimates are computed using (48) of the main paper. The data were simulated using a single group model with the power law network. The mean number of contacts is $k = 10$. The exposure intensity parameter is $\tau_t = \beta_t/k$. Population size is $n = 10,000$.

S5 Calibration and counterfactual analyses

In this section, we provide additional results for the calibration and counterfactual exercises described in the paper. Figure S.6 shows that $\hat{\mathcal{R}}_{et} = (1 - \text{MF}c_t)\,\hat{\beta}_t/\gamma$ is almost the same as $\hat{\beta}_t/\gamma$ since the proportion of infected is very small even after taking account of under-reporting. As infected cases have grown, small differences between $\hat{\beta}_t/\gamma$ and $\hat{\mathcal{R}}_{et}$ start to become visible towards the end of our sample period (mid-October). Figure S.7 shows that the 2-weekly and 3-weekly rolling estimates of the effective reproduction numbers using realized data, are very close to each other for all six countries under consideration. Therefore, our findings would be similar if we adopt the 2-weekly rolling estimates of β_t in calibrating the model to the empirical evidence.

To complement the counterfactuals presented in the main paper if the German (UK) lockdown were delayed (brought forward) one week, we further examine the potential outcomes if the lockdown were delayed or advanced two weeks. As shown in Figure S.8, if the German lockdown had been delayed one week, there would have been a whopping five-fold increase in both infected and active cases. By contrast, if the UK lockdown had been implemented two weeks earlier, both infected and active cases could have been one-fifth of the realized level. These results further highlight the importance of taking mitigation actions early in an epidemic outbreak.

Figure S.6: Comparison of $\hat{\mathcal{R}}_{et}$ and $\hat{\beta}_t/\gamma$ for selected European countries

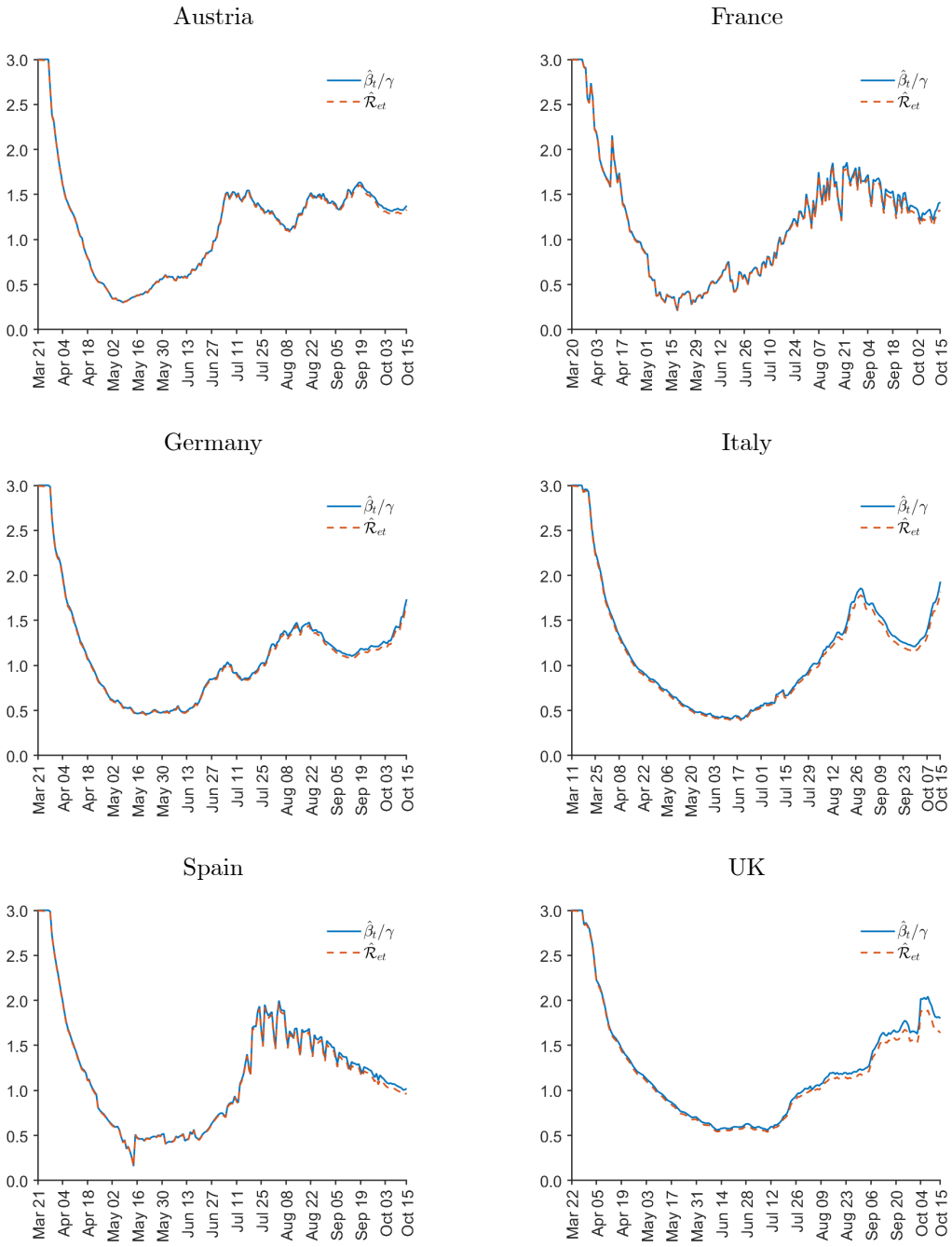

Notes: $\hat{\beta}_t$ is the 3-weekly rolling estimate of β_t computed using (48) of the main paper. $\hat{\mathcal{R}}_{et} = (1 - \text{MF}c_t)\,\hat{\beta}_t/\gamma$, where $\gamma = 1/14$ and the value of MF for each country is given in Figure 8 of the main paper. The number of removed (recoveries + deaths) is estimated recursively using $R_t = (1-\gamma)\,R_{t-1} + \gamma C_{t-1}$ for all countries, with $C_1 = R_1 = 0$. To render the calibrations comparable across the six countries, β is set to 3/14 (giving $\mathcal{R}_0 = 3$) during the first week of the epidemic.

Figure S.7: Rolling estimates of the effective reproduction numbers ($\mathcal{R}_{et}$) under 2- and 3-weekly rolling windows for selected European countries

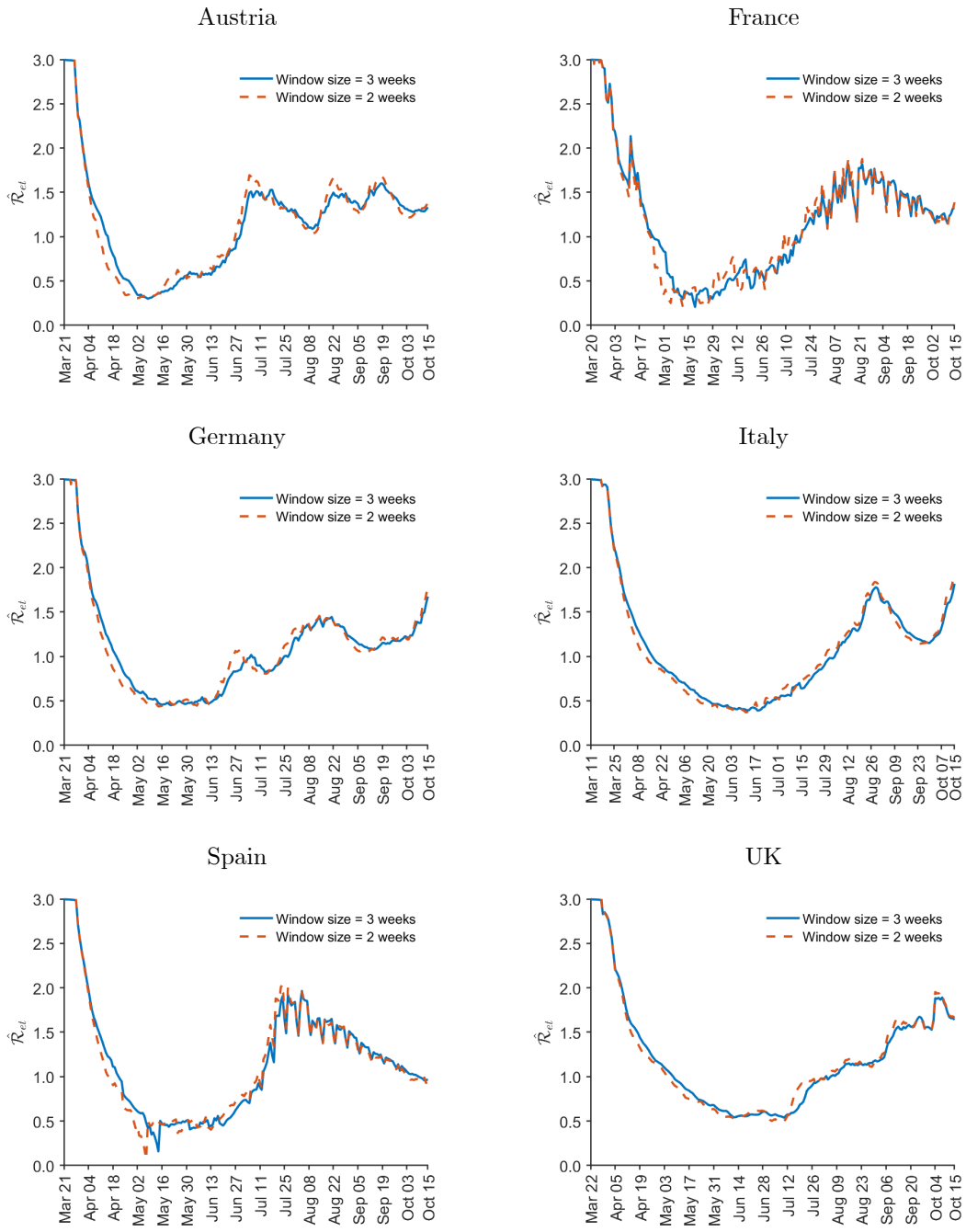

Notes: $\hat{\mathcal{R}}_{et} = (1 - \text{MF}c_t)\,\hat{\beta}_t/\gamma$, where $\gamma = 1/14$ and the value of MF for each country is given in Figure 8 of the main paper. The rolling estimates of β_t are computed using (48) of the main paper. The number of removed (recoveries + deaths) is estimated recursively using $R_t = (1-\gamma)\,R_{t-1} + \gamma C_{t-1}$ for all countries, with $C_1 = R_1 = 0$. To render the calibrations comparable across the six countries, β is set to 3/14 (giving $\mathcal{R}_0 = 3$) during the first week of the epidemic.

Figure S.8: Counterfactual number of infected and active cases for Germany and UK under different lockdown scenarios

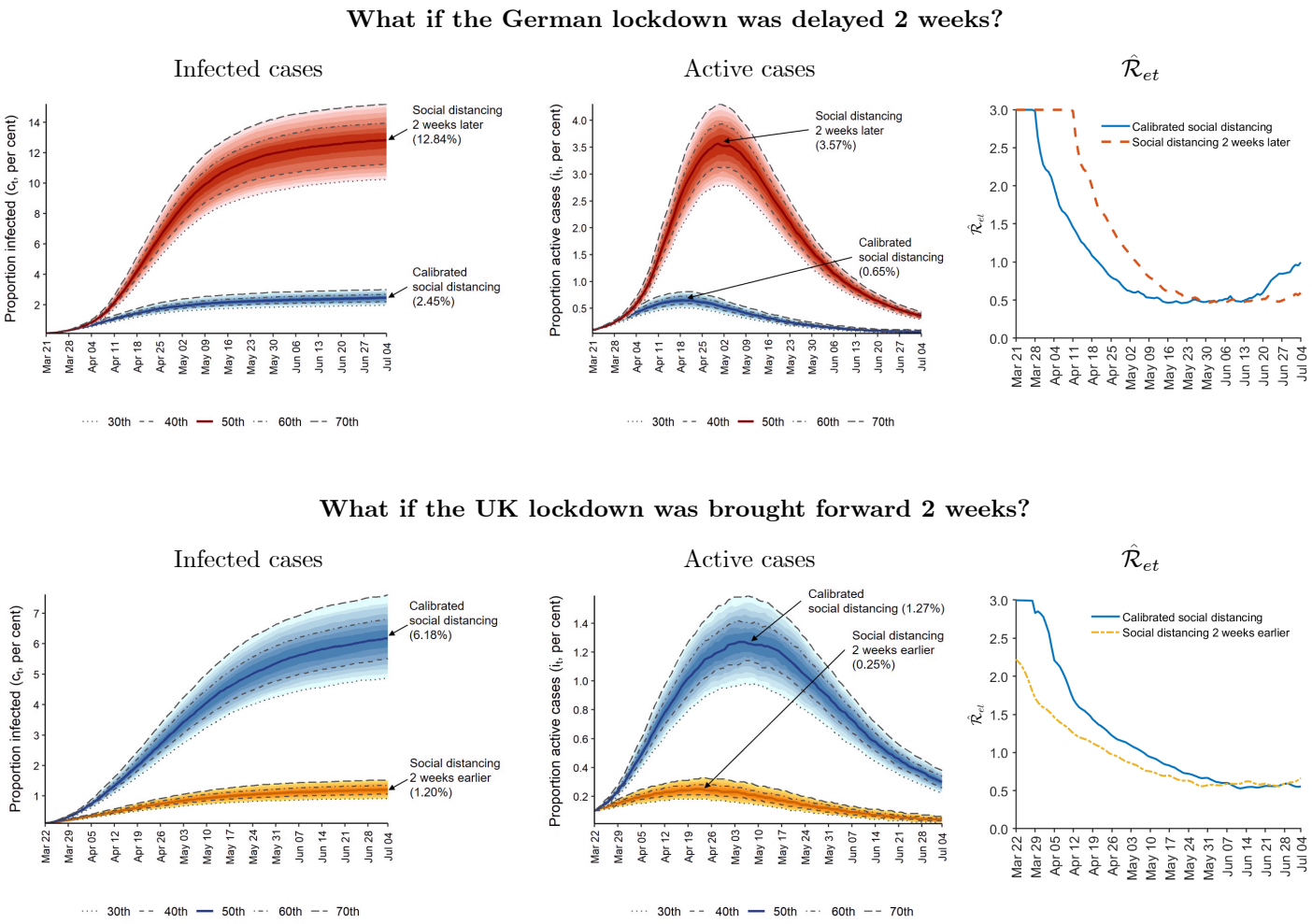

Notes: The simulation uses a single group model with power law network and begins with 1/1000 of the population randomly infected in day 1. $n = 10,000$. $k = 10$. $\gamma = 1/14$. $\hat{\tau}_t = \hat{\beta}_t/k$, where $\hat{\beta}_t$ is the 3-weekly rolling estimate computed using (48). The number of removed (recoveries + deaths) is estimated recursively using $R_t = (1-\gamma)\,R_{t-1} + \gamma C_{t-1}$ for both countries, with $C_1 = R_1 = 0$. The median of $\hat{\mathcal{R}}_{et}^{(b)} = \left(1 - c_t^{(b)}\right)\hat{\beta}_t/\gamma$ over 1,000 replications is displayed in the last column.